CRB3 navigates Rab11 trafficking vesicles to promote γTuRC assembly during ciliogenesis

Bo Wang[1, 2, †], Zheyong Liang[1, 3, †], Tan tan[4], Miao Zhang[1, 2], Yina Jiang[5], Yangyang Shang[1, 2], Xiaoqian Gao[1, 2], Shaoran Song[1, 2], Ruiqi Wang[1, 2], He Chen[1, 2], Jie Liu[1, 2], Juan Li[1, 2], Yu Ren[6], and Peijun Liu[1, 2] *

[1]Center for Translational Medicine, the First Affiliated Hospital of Xi'an Jiaotong University, Xi'an 710061, Shaanxi, P.R. China.

[2]Key Laboratory for Tumor Precision Medicine of Shaanxi Province, the First Affiliated Hospital of Xi'an Jiaotong University, Xi'an 710061, Shaanxi, P.R. China.

[3]Department of Cardiovascular Surgery, the First Affiliated Hospital of Xi'an Jiaotong University, Xi'an 710061, Shaanxi, P.R. China.

[4]Center for Precision Medicine, Affiliated to The First People's Hospital of Chenzhou, University of South China, Chenzhou 423000, Hunan, P.R. China.

[5]Department of Pathology, the First Affiliated Hospital of Xi'an Jiaotong University, Xi'an 710061, Shaanxi, P.R. China.

[6]Department of Breast Surgery, the First Affiliated Hospital of Xi'an Jiaotong University, Xi'an 710061, Shaanxi, P.R. China.

† These authors contributed equally to the work.

* Correspondence:

Peijun Liu

E-mail: liupeijun@xjtu.edu.cn

Running Title: CRB3 regulates ciliogenesis

Keywords: Primary cilium, Polarity protein, Breast cancer, CRB3, γ-TuRC assembly, Rab11-positive endosome

Abstract

The primary cilium plays important roles in regulating cell differentiation, signal transduction, and tissue organization. Dysfunction of the primary cilium can lead to ciliopathies and cancer. The formation and organization of the primary cilium are highly associated with cell polarity proteins, such as the apical polarity protein CRB3. However, the molecular mechanisms by which CRB3 regulates ciliogenesis and CRB3 location remain unknown. Here, we show that CRB3, as a navigator, regulates vesicle trafficking in γ-TuRC assembly during ciliogenesis and cilium-related Hh and Wnt signaling pathways in tumorigenesis. *Crb3* knockout mice display severe defects of the primary cilium in the mammary ductal lumen and renal tubule. CRB3 is essential for lumen formation and ciliary assembly in the mammary epithelium. We demonstrate that CRB3 localizes to the basal body and that CRB3 trafficking is mediated by Rab11-positive endosomes. Significantly, CRB3 directly interacts with Rab11 to navigate GCP6/Rab11 trafficking vesicles to CEP290, resulting in intact γ-TuRC assembly. In addition, CRB3-depleted cells cannot respond to the activation of the Hh signaling pathway, while CRB3 regulates the Wnt signaling pathway. Therefore, our studies reveal the molecular mechanisms by which CRB3 recognizes Rab11-positive endosomes to navigate apical vesicle trafficking in effective ciliogenesis, maintaining cellular homeostasis and tumorigenesis.

Introduction

Epithelial tissues are the most common, widely distributed, and perform several particular functions. The integrity of the specific cellular architecture composed of epithelial cells is necessary for these functions of epithelial tissues. Establishing apical-basal cell polarity within epithelial cells is a crucial biological process for epithelial homeostasis. Most human cancers originate from epithelial tissues, and loss of apical-basal cell polarity is one of the most significant hallmarks of advanced malignant tumors[1]. Several reports have shown that loss of some polarity proteins causes disordered cell polarity within epithelial cells, which cannot tightly control cellular growth and migration, ultimately leading to tumor formation, progression,

and metastasis[2, 3]. However, the relationship between polarity proteins and tumorigenesis remains incomplete.

The crumb complex, located apically, is vital in regulating and maintaining apical-basal cell polarity within epithelial cells. In mammals, three Crumbs orthologs are CRB1, CRB2, and CRB3, and only CRB3 is widely expressed in epithelial cells[4]. Our previous studies have shown that CRB3 is expressed at low levels in renal and breast cancers, and abnormal CRB3 expression leads to the disrupted organization of MCF10A cells in three-dimensional (3D) cultures[5-7]. Inhibition of CRB3 impairs contact inhibition and leads to migration, invasion and tumorigenesis of cancer cells[6, 8]. The contact inhibition results in growth arrest and causes epithelial cells to enter the quiescent phase, inducing primary cilium formation.

The primary cilium, an antenna-like microtubule-based organelle in most types of mammalian cells, is a sensorial antenna that regulates cell differentiation, proliferation, polarity, and tissue organization[9]. Dysfunction of the primary cilium can lead to developmental and degenerative disorders called ciliopathies, such as polycystic kidney disease, nephronophthisis, retinitis pigmentosa, and Meckel syndrome[10]. Remarkably, it has been reported that many cancers, including melanoma and breast, renal, pancreatic, and prostate cancer, exhibit loss of the primary cilium, most likely during the early stages of tumorigenesis[11-15]. The primary cilium is a significant extension on the apical surfaces of epithelial cells and is maintained by polarized vesicular traffic[16]. Some studies have shown that CRB3 localizes in the primary cilium and that depletion of CRB3 leads to primary cilium loss in Madin-Darby canine kidney (MDCK) cells[17, 18], indicating that CRB3 is necessary for the initiation of ciliogenesis. However, how CRB3 promotes ciliogenesis on the apical surfaces of epithelial cells remains unknown.

Here, we describe a novel conditional deletion of *Crb3* in mice and show that Crb3 is required to assemble the primary cilium in the gland, kidney and MEF cells from *Crb3* knockout mice and that *Crb3* deletion promotes breast cancer progression *in vivo*. We found that CRB3, which directly interacts with Rab11, navigates GCP6/Rab11 trafficking vesicles to the basal body of the primary cilium in mammary

epithelial cells. Additionally, we identified that CRB3 regulates the ciliary Hedgehog (Hh) and Wnt signaling pathways in breast cancer. Thus, we found unexpected diversity in the polarity protein CRB3 navigating polarized Rab11-dependent traffic, leading to a novel assembly mechanism of the γ-tubulin ring complex (γTuRC) in ciliogenesis.

Results

Crb3 deletion mice exhibit smaller and anophthalmia.

Since *Crb3* knockout mice die shortly after birth[19], we generated a novel transgenic mouse model with conditional deletion of *Crb3* using the Cre-loxP system. The loxP sites flanked either side of exon 3 in the *Crb3* gene (Supplementary Fig. 1A). The positive embryonic stem (ES) cell clone was confirmed for the wild-type gene ($Crb3^{wt/wt}$) and recombinant allele ($Crb3^{wt/fl}$) by Southern blotting (Supplementary Fig. 1B). The genotypes of the wild type, heterozygotes and homozygotes ($Crb3^{fl/fl}$) were detected with specific primers (Supplementary Fig. 1C). We first intercrossed $Crb3^{fl/fl}$ with CMV enhancer/chicken β-actin promoter (CAG)-Cre mice and found that $Crb3^{fl/fl}$, $Crb3^{wt/fl}$; CAG-Cre and $Crb3^{fl/fl}$; CAG-Cre pups were born normally and looked well developed in size. However, most $Crb3^{fl/fl}$; CAG-*Cre* pups died within a few days after birth. Few surviving $Crb3^{fl/fl}$; CAG-*Cre* mice were smaller and showed anophthalmia than littermate $Crb3^{fl/fl}$ mice at 4 weeks old (Fig. 1A-B). The eye is an organ with perfect apical-basal cell polarity. However, *Crb3* knockout mice showed ocular abnormalities. Together, these results indicated that Crb3 is necessary for eye development.

Mammary epithelial-specific *Crb3* deletion causes ductal epithelial hyperplasia and tumorigenesis.

Based on our earlier studies showing that inhibition of CRB3 impairs the organization of breast epithelium, we set out to directly explore the role of Crb3 in mammary gland development. We first developed epithelial cell-specific deletion of *Crb3* in the mammary gland by intercrossing $Crb3^{fl/fl}$ mice with mouse mammary tumor virus long terminal repeat promoter (MMTV)-*Cre* mice. We demonstrated the expression of

121 Crb3 in the mammary gland using immunoblotting, real-time quantitative PCR, and
122 immunohistochemistry, and the level of Crb3 expression was deficient in mammary
123 epithelial cells with Crb3 knockout (Supplementary Fig. 1D-F).
124 To assess the function of Crb3 in the development of mammary epithelial cells, we
125 analyzed whole mammary mounts from 8-week-old virgin *Crb3*$^{fl/fl}$;MMTV-*Cre* and
126 littermate *Crb3*$^{fl/fl}$ mice. *Crb3*$^{fl/fl}$;MMTV-*Cre* mice displayed significantly increased
127 numbers of terminal end buds (TEBs) and bifurcated TEBs than *Crb3*$^{fl/fl}$ mice (Fig. 1
128 C-E). The histopathology results showed that normal ductal epithelial cells were
129 arranged as a monolayer in *Crb3*$^{fl/fl}$ mice, while *Crb3* knockout led to ductal epithelial
130 hyperplasia with increased ductal thickness in *Crb3*$^{fl/fl}$;MMTV-*Cre* mice (Fig. 1 F).
131 To observe the role of Crb3 in the tumorigenesis of breast cancer, we observed
132 mammary glands from 9-week-old virgin polyomavirus middle T antigen
133 (PyMT)-cKO-Crb3 and PyMT-WT mice whose mammary glands progressed to early
134 carcinomas and lost their normal epithelial architecture[20]. The PyMT mouse model
135 has been widely used in the study of tumor initiation and development with similar
136 histological progression to human breast cancer. PyMT-WT mice exhibited loss of
137 epithelial features and development of breast cancer, while PyMT-cKO-Crb3 mice
138 grew larger tumors with faster tumor progression and a poorly differentiated
139 phenotype (Fig. 1G). Thus, Crb3 knockout leads to ductal epithelial hyperplasia and
140 promotes tumorigenesis, and it is essential for branching morphogenesis in mammary
141 gland development and tumor progression.
142 **CRB3 knockdown inhibits lumen formation in acini of mammary epithelial cells.**
143 MCF10A cells are spontaneously immortalized human breast epithelial cells with the
144 characteristics of normal breast epithelium[21]. MCF-10A cells could form acini
145 similar to mammary epithelial acini under 3D basement membrane culture conditions.
146 It has become a valuable system to study the morphogenesis and oncogenesis of the
147 mammary epithelium[22]. To confirm the function of CRB3 in mammary epithelial
148 acini formation, we first knocked down the expression of CRB3 by lentiviral shRNA
149 in MCF10A cells (Supplementary Fig. 2A and B). Under the 3D culture system, we
150 found that MCF10A cells infected with no target shRNA lentivirus could form acini

151 after 6 days (D6) and finally formed polarized acini with a hollow lumen at D14 (Fig.
152 2A). However, MCF10A cells, after CRB3 knockdown, formed more number, larger
153 diameter and aberrant acini after D6, and these acini had no lumen (Fig. 2A-D). Cell
154 proliferation assays of MCF10A cells showed that CRB3 knockdown increased the
155 proliferation rate and accelerated G1 to S phase progression (Supplementary Fig.
156 2C-E).
157 Apoptosis and mitotic spindle orientation during lumen formation were further
158 investigated in a 3D culture system. The immunofluorescence (IF) results showed that
159 more internal cleaved-caspase 3-positive acini were observed in the control groups
160 than in the CRB3 knockdown groups at D9 (Fig. 2E). CRB3 overexpression
161 significantly promoted apoptosis in breast cancer cells (Supplementary Fig. 2F-H).
162 Similarly, the staining of α-tubulin in mitotic cells exhibited more misorientation of
163 the mitotic spindle in CRB3 knockdown groups (Fig. 2F-H).
164 In addition to verifying the effect of *Crb3* deletion on promoting proliferation and
165 inhibiting apoptosis *in vivo*, these markers were detected in primary tumor tissue from
166 PyMT-WT and PyMT-cKO-Crb3 mice. *Crb3* deletion increased the numbers of
167 proliferative and mitotic cells and decreased the numbers of apoptotic cells in primary
168 tumors (Fig 2I). These results demonstrate that CRB3 could promote the proliferation
169 of mammary epithelial cells, disturb the mitotic spindle orientation, and protect the
170 internal cells from apoptosis during acini formation, finally leading to irregular lumen
171 formation and tumor progression.
172 **CRB3 regulates primary cilium formation.**
173 The primary cilium, one of the apical antenna-like extensions in epithelial cells, has
174 been reported to play an important role in controlling lumen formation[23]. CRB3
175 knockdown leads to primary cilium loss in MDCK cells[17, 18], but the molecular
176 mechanism regulating ciliogenesis on apical surfaces is still unclear. Investigating the
177 altered effect of CRB3 on ciliogenesis *in vivo* and *in vitro*, we found that control
178 MCF10A cells formed primary cilia after becoming confluent, while CRB3
179 knockdown led to significant ciliogenesis defects (Fig. 3A). Compared with the
180 control, the number of cells with primary cilium was significantly increased, and the

181 length of the existing primary cilium was not different (Fig. 3B). Conversely, CRB3
182 conditional overexpression, adding doxycycline (+dox), resulted in restoring ciliary
183 assembly in MCF7 cells (Fig. 3C). CRB3 overexpression increased the proportion of
184 primary cilium formation in breast cancer cells, and the length of the restored primary
185 cilium was increased (Fig. 3D). Importantly, the primary cilium could be directly
186 visualized using scanning electron microscopy (SEM) (Fig. 3E). MCF10A cells with
187 primary cilia were significantly decreased after CRB3 knockdown, while CRB3
188 conditional overexpression did not increase these populations (Fig. 3F).
189 To further corroborate these findings *in vivo*, we used breast and kidney tissue to
190 assess ciliogenesis in the *Crb3* knockout mouse model. Renal epithelial cells can form
191 prominent primary cilia, and the absence of primary cilia leads to ciliopathies. We
192 used immunofluorescence to detect ciliary formation in the mammary ductal lumen
193 and renal tubule. Compared with tissues of *Crb3*$^{fl/fl}$ mice, *Crb3* knockout led to the
194 absence of primary cilium in the mammary ductal lumen and renal tubule from
195 *Crb3*$^{fl/fl}$; CAG-*Cre* mice (Fig. 3G, H). In particular, the proportion of cells forming the
196 primary cilium plummeted (Fig. 3G, H). This same phenomenon was also observed in
197 mouse embryonic fibroblasts (MEFs) from *Crb3*$^{fl/fl}$; CAG-*Cre* mice (Supplementary
198 Fig. 3A, B). We conclude that CRB3 plays a central role in ciliogenesis in various
199 tissues and mammary cells.
200 **CRB3 localizes to the basal body of the primary cilium.**
201 CRB3, a polarity protein, was mostly reported to be localized on the tight junctions of
202 the apical epithelium membrane[24]. Additionally, we noted that CRB3 could be
203 closely colocalized with centrosomes at prophase, metaphase, and anaphase[17]. To
204 investigate the relationship between CRB3 and ciliary formation, we first examined
205 CRB3 localization in MCF10A cells that expressed CRB3-GFP. In MCF10A cells,
206 exogenous CRB3 was mainly localized at cell tight junctions and could colocalize
207 with pericentrin (a centrosome marker) (Fig. 4A). And approximately 40% of cells
208 had this co-localization of exogenous CRB3 and pericentrin (Fig. 4B). We observed
209 the localization of endogenous CRB3 with another centrosome marker to verify this
210 phenomenon. Similarly, we detected that CRB3 accumulated on one side of the

211 cytoplasm and had a CRB3 focous located at the basal body represented by γ-tubulin
212 in MCF10A cells (Fig. 4C, D). Importantly, CRB3 knockdown disturbed the
213 accumulation of γ-tubulin at the basal body in the confluent quiescence cells (Fig. 4C).
214 To demonstrate the relationship of this colocalization to the primary cilium, we
215 employed acetylated tubulin to mark the primary cilium. Double immunostaining
216 showed that this CRB3 focous was the basal body of the primary cilium, and CRB3
217 knockdown inhibited ciliary assembly in MCF10A cells (Fig. 4E, F). These results
218 suggest that CRB3 is located at the basal body of the primary cilium and that CRB3
219 knockdown disturbs the accumulation of γ-tubulin in quiescent cells.

220 **CRB3 trafficking is mediated by Rab11-positive endosomes.**

221 To better investigate the molecular mechanisms of CRB3 in regulating primary cilium
222 formation, we detected a series of genes related to ciliogenesis, including markers of
223 centriole or primary cilium, basal body (BB) components, intraflagellar transport
224 (IFT)-A and IFT-B anterograde transport. However, CRB3 knockdown did not alter
225 the mRNA expression of these genes (Supplementary Fig. 4A). Then, we carried out
226 coimmunoprecipitation (co-IP) tandem mass spectrometry using tagged exogenous
227 CRB3 as bait to identify its interacting proteins (Supplementary Fig. 4B). Pathway
228 aggregation analysis of these proteins revealed that these interacting proteins of CRB3
229 were significantly involved in Golgi vesicle transport and vesicle organization (Fig.
230 5A). We focused on these pathways because smaller distal appendage vesicle (DAV)
231 formation is critical for ciliogenesis initiation, and it requires the Rab GTPase
232 Rab11-Rab8 cascade to function[25]. Interestingly, some Rab small GTPase family
233 members identified as CRB3-binding proteins were aggregated in these pathways,
234 such as Rab10, Rab11A, Rab11B, Rab14, Rab1A, Rab1B, Rab21, Rab2A, Rab32,
235 Rab35, Rab38, Rab5B, Rab5C, and Rab6A. Several centriolar proteins were also
236 identified, including tubulin gamma-1, tubulin gamma-2, CENP-E, CEP290, CEP192,
237 CEP295, and CEP162 (Fig. 5B).

238 Rab11-positive vesicles bind to centrosomal Rabin8, leading to ciliary membrane
239 formation[26]. This report suggested that the trafficking of Rab11-positive vesicles
240 and polarized vesicles is an essential process for early ciliary assembly. Next, we

241 examined the polarized vesicle traffic of CRB3 in MCF10A cells. Our studies found
242 that CRB3 could colocalize with EEA1-positive early endosomes, CD63-positive late
243 endosomes and Rab11-positive recycling endosomes (Fig. 5C). In addition, after 2
244 hours of treatment with dynasore, an endocytosis inhibitor, CRB3 significantly
245 accumulated at the cytomembrane, and the colocalization of CRB3 with EEA1-,
246 CD63-, and Rab11-positive endosomes was significantly decreased (Fig. 5C, D). We
247 have reported that CRB3 expression correlates with the contact-dependent change,
248 which is CRB3 expression reduced considerably in confluent MCF10A cells[6]. Then,
249 dynasore could also rescue the CRB3 downregulation induced by the increasing cell
250 density of MCF10A cells (Fig. 5E). CRB3 knockdown did not affect Rab11
251 expression (Supplementary Fig. 4C). These results suggest that the intracellular
252 trafficking of CRB3 is mediated by Rab11-positive endosomes at different cell
253 densities.

254 **CRB3 knockdown destabilizes γTuRC assembly during ciliogenesis.**

255 According to our findings, we assumed that CRB3 might play an important role in
256 polarized vesicle trafficking. The γ-Tubulin ring complex (γTuRC) is a central
257 regulator of microtubule nucleation and is a nucleation site of α-Tubulin and
258 β-Tubulin at the microtubule-organizing center in mitotic cells[27]. The primary
259 cilium is a microtubule-based structure attached to the basal body transformed from
260 the mother centriole. As we found that CRB3 knockdown disturbed the accumulation
261 of γ-tubulin, we analyzed γTuRC assembly in ciliogenesis. The γTuRC is composed
262 of multiple copies of the γ-tubulin small complex (γTuSC), GCP2 and GCP3, plus
263 GCP4, GCP5, and GCP6[27, 28] (Fig. 5F). CRB3 downregulation did not affect the
264 expression of γTuRC subunits (Fig. 5G). Then, we performed co-IPs directed against
265 GCP6 in CRB3-depleted cells and assessed the relative levels of both γTuSC-specific
266 proteins compared with the control shRNA-treated cells. Interestingly, CRB3
267 knockdown significantly reduced the interaction of GCP6 with GCP3 (Fig. 5H). To
268 verify this phenomenon, we observed the localization of GCP3 with GCP6 foci in
269 MCF10A cells. Correspondingly, CRB3 downregulation significantly disturbed the
270 colocalization of GCP3 with GCP6 foci in quiescence cells (Fig. 5I). To investigate

271 whether CRB3 facilitate γTuRC assembly, we fractionated MCF10A cytoplasmic
272 proteins on sucrose gradients according to the method published[29]. We noticed that
273 γTuSC were regimented mainly in fractions 3 and γTuRC sediment in fractions 6 (Fig.
274 5J). However, CRB3 downregulation caused most of GCP6 and GCP5 to be
275 precipitated independently of γTuRC in the low-density fractions (Fig. 5J). Together,
276 these results have established that the depletion of CRB3 interferes with the molecular
277 interactions between the γTuRC proteins, failing microtubule formation in the primary
278 cilium. However, it may not affect the expression of these molecules during γTuRC
279 assembly. According to these results, we hypothesized that CRB3 could mediate the
280 polarized vesicle trafficking of some γTuRC-specific proteins during Rab11-positive
281 endosomes.

282 **CRB3 directly interacts with Rab11.**

283 To fully prove this hypothesis, we first examined CRB3 interaction with
284 Rab11-positive endosome and γTuRC-specific proteins in MCF10A cells. Using
285 CRB3 as bait, we identified that CRB3 could interact with Rab11 instead of GCP6
286 and GCP3 (Fig. 6A). In contrast, Rab11 could interact with CRB3 and GCP6 instead
287 of GCP3 by tagging Rab11 as bait (Fig. 6B). Thus, does CRB3 knockdown affect the
288 trafficking of γTuRC-specific proteins during Rab11-positive vesicles? The co-IP
289 results showed that CRB3 knockdown did not affect Rab11 interacting with GCP6,
290 and the level of Rab11 binding to GCP6 had a tendency to decrease in MCF10A cells
291 with CRB3 knockdown (Fig. 6C). The colocalization rate of Rab11 and GCP6 was
292 significantly decreased in MCF10A cells with CRB3 knockdown (Supplementary Fig.
293 5A-C). Consistent with other reports[30], Rab11 knockdown significantly inhibited
294 primary cilium formation in MCF10A cells (Supplementary Fig. 5D-F).

295 Based on these results, we further detected the region of CRB3 interacting with Rab11
296 by using coexpression and co-IP in HEK293 cells. CRB3 consists of a signal peptide
297 (SP), extracellular domain, transmembrane (TM), FERM-binding domain (FBD), and
298 carboxy-terminal PDZ-binding domain (PBD). Due to the specificity of the C- and
299 N-terminal domains, we constructed CRB3-GFP fusion proteins where GFP tags were
300 fused to the extracellular domain as previously reported[31] (Fig. 6D). According to

301 these domains, we also constructed the truncations of CRB3-GFP fusion proteins with
302 serial C-terminal deletions (Fig. 6E) and another Flag-Rab11a fusion protein. The
303 coexpression and co-IP results showed that Flag-Rab11a interacted with full-length
304 CRB3 (1-120), CRB3 (1-116), CRB3 (1-83), and CRB3 (1-58) but not CRB3 (1-26)
305 (Fig. 6F). Therefore, the region of CRB3 interacting with Rab11 is amino acids 27 to
306 58.
307 Rab11, a small GTP-binding protein, is an essential regulator of the dynamics in
308 recycling endosomes, which are required to undergo GDP/GTP cycles. In particular,
309 Rab11a[S25N] is a GDP-locked form, Rab11a[S20V], and Rab11a[Q70L] is a
310 GTP-locked form[30]. To further investigate the GTP-bound form of Rab11a
311 interacting with CRB3, we constructed these mutant variants of Rab11a. Next, we
312 found that the weaker interaction of CRB3 and these mutant variants, Rab11a[Q70L],
313 Rab11a[S20V] and Rab11a[S25N], compared with Rab11aWT, was observed using
314 co-IP analysis (Fig. 6G). Together, these results indicate that CRB3 directly interacts
315 with Rab11a, depending on the GTPase activity of Rab11a.
316 **CRB3 navigates GCP6/Rab11 trafficking vesicles to CEP290 in the primary**
317 **cilium.**
318 Since CRB3 knockdown does not affect the interaction with Rab11-positive
319 endosome and γTuRC-specific proteins GCP6, we wanted to know whether CRB3
320 affected the localization of GCP6/Rab11 trafficking vesicles to the basal body of the
321 primary cilium. Reviewing the identification of CRB3 interacting proteins, there are
322 some centriolar proteins. CEP290 is located in the transition zone of the primary
323 cilium and is required for the formation of microtubule-membrane linkers[32]. Then,
324 we verified that exogenous CRB3 could bind to CEP290, Rab11, GCP6 (Fig. 7A), and
325 Rab11 also interacted with CEP290, CRB3-GFP, GCP6 (Fig. 7B). Similar to Fig. 6C,
326 the amount of GCP6 bonded to Rab11 was reduced within CRB3 knockdown.
327 Importantly, CRB3 knockdown showed that Rab11 hardly bonded to CEP290 (Fig.
328 7C). We checked the colocalization of the basal body foci of GCP6 and γ-tubulin,
329 γ-tubulin and Rab11 in MCF10A and MEF cells to corroborate this result. In
330 quiescence control cells, GCP6 foci and γ-tubulin formed a prominent focus at the

basal body of the primary cilium, as observed by immunofluorescence. However, CRB3 downregulation eliminated this focus and significantly disturbed the basal body foci of GCP6 and γ-tubulin in MCF10A cells (Fig. 7D), and γ-tubulin and Rab11 in MEF cells (Fig. 7E). At the beginning of this experiment, we also tried to show the interaction of CRB3, Rab11 and GCP6 with expressing fluorescence tagged GCP6 protein and FRET assay. However, the centrosomal foci of fluorescent GCP6 was difficult to capture because of too weak signal, and this may require re-overexpression of ninein-like protein (Nlp) to promote γTuRC enrichment[29, 33].

Although CRB3 knockdown had little effect on the formation of GCP6/Rab11 trafficking vesicles, it could significantly inhibit the γTuRC assembly during ciliogenesis, thus affecting the transport of GCP6/Rab11 trafficking vesicles to the basal body of the primary cilium. Since CRB3 affected the combination of Rab11 and CEP290, we speculate that CRB3 could be a navigator, navigating GCP6/Rab11 trafficking vesicles to the basal body of the primary cilium.

CRB3 regulates the Hh and Wnt signaling pathways in tumorigenesis

To examine the role of CRB3 in regulating ciliary assembly in breast cancer, we explored the relationship between CRB3 and the primary cilium in breast cancer tissues. We found that CRB3 was localized at the subapical surface of the mammary gland lumen in the paracarcinoma tissues. CRB3 had no obvious expression or localization in breast cancer tissues (Fig. 8A). The immunofluorescence analysis results showed that the intact primary cilium could be observed in the adjacent para-carcinoma tissues, whereas the number of cells with primary cilia was much lower in breast cancer tissues (Fig. 8B, C). Consistent with previous findings, CRB3 was localized at the basal body of the primary cilium in adjacent para-carcinoma tissues (Fig. 8D). These results again suggest that a defect in CRB3 expression inhibits ciliary assembly, which could be involved in tumorigenesis.

To detect some functional consequences of the absence of the primary cilium, we measured alterations in the Hedgehog (Hh) and Wnt signaling pathways in CRB3-depleted cells. We first detected the translocation of SMO into the primary cilium and the expression of the target gene GLI1. SAG is a potent Smoothened

361 (SMO) receptor agonist that activates the Hh signaling pathway. CRB3 knockdown
362 did not promote the translocation of SMO into the primary cilium in MCF10A cells
363 treated with SAG (Fig 8E). After SAG treatment, the mRNA expression of GLI1 was
364 significantly decreased in CRB3-depleted cells (Fig 8F). Crb3 knockout did not alter
365 the expression or cellular localization in primary tumors from PyMT-cKO-Crb3 mice
366 (Fig 8H). We have reported that CRB3 expression was high in immortalized
367 mammary epithelial cells while loss of CRB3 expression in breast cancer cells[6]. On
368 the other hand, western blotting results showed that GSK3-β was significantly
369 downregulated after CRB3 knockdown in MCF10A cells. In addition, β-catenin, the
370 major effector of the canonical Wnt signaling pathway, was upregulated. CRB3
371 overexpression resulted in upregulation of GSK3-β and downregulation of β-catenin
372 in breast cancer cells (Fig. 8G). Visibly, β-catenin was significantly upregulated and
373 markedly localized in the nucleus from PyMT-cKO-Crb3 mice (Fig 8I). Together,
374 these data suggest that CRB3 knockdown cannot activate the Hh signaling pathway
375 but can activate the Wnt signaling pathway, which is ultimately involved in
376 tumorigenesis.
377
378 **Discussion**
379 Apical-basal cell polarity is essential for cellular architecture, development and
380 homeostasis in epithelial tissues. Most malignant cancers lack cell polarity because of
381 the unconstrained cell cycle and cell migration with decreased adhesion. CRB3, an
382 important apical protein, is significantly reduced in various tumor cells and tissues
383 and promotes metastasis and tumor formation in nude mice[5, 6, 8, 34-36]. Here, we
384 generate a novel transgenic mouse model with conditional deletion of Crb3 to study
385 the role of polarity proteins in tumorigenesis. *Crb3* knockout mice were reported to
386 have cystic kidneys, improper airway clearance in the lung, villus fusion, apical
387 membrane blebs, and disrupted microvilli in intestine airway clearances, which
388 demonstrated that CRB3 is crucial for the development of the apical membrane and
389 epithelial morphogenesis[19, 37]. Importantly, our studies in the *Crb3* knockout
390 mouse model suggest that in addition to death after birth, it is characterized by smaller

size, ocular abnormality, bronchial smooth muscle layer defect, reduced pancreatic islets and hyperplasia mammary ductal and renal tubular epithelium (some data not shown). These important phenotypic changes are due to disruption of epithelial polarity homeostasis, which may ultimately lead to tumorigenesis.

In addition, we also found the absence of primary cilia in the mammary ductal lumen and renal tubule in the *Crb3* knockout mouse model. Consistent with other reports, CRB3 knockdown regulated ciliary assembly in MDCK cells[17, 18]. Furthermore, CRB3 was localized in the inner segments of photoreceptor cells and concentrated with the connecting cilium during the whole development of the mouse retina[38]. These ocular defect phenotypes remarkably resemble EHD1 knockout mice, which regulate ciliary vesicle formation in primary cilium assembly[25, 39, 40]. Hence, CRB3 can affect primary cilium formation in various epithelial tissues, such as the breast, kidney, and retina.

Previous literature has reported that CRB3 localizes in the primary cilium in differentiated MDCK cells[17, 18], but we mainly found that it is not located on the basal body of the primary cilium in mammary epithelial cells. The immunofluorescence results in these literatures showed that CRB3 was scattered on the primary cilia, and had a strong foci at the basal body. Especially in rat kidney collecting ducts, the localization of CRB3 on primary cilia was significantly reduced, while the obvious localization was basal body[18]. Another literature also reported the co-localization of CRB3 and γ-tubulin in MDCK cells[17]. This result is consistent with our conclusion, and we also verified its co-localization with centrosome by overexpressing CRB3 in mammary epithelial cells, indicating that CRB3 mainly localized to the basal body of the primary cilium. Given that CRB3 also alters primary cilium formation in the mammary epithelium, it is important to investigate the molecular mechanisms by which CRB3 regulates primary cilium formation.

Polarized vesicular traffic plays an important role in extending the primary cilium on apical epithelial surfaces, and the molecular mechanism and relationship to tumorigenesis remain unclear. Here, we reveal that Rab11-positive endosomes mediate the intracellular trafficking of CRB3 and that CRB3 can navigate

421 GCP6/Rab11 trafficking vesicles to CEP290 for correct γTuRC assembly during
422 primary cilium formation. Moreover, in the presence of CRB3, the epithelium can
423 form contact inhibition and an intact primary cilium in quiescence to achieve cellular
424 homeostasis. In contrast, loss of contact inhibition and primary cilium formation with
425 CRB3 deletion can activate the Wnt signaling pathway, affect the Hh signaling
426 pathway, and disrupt the imbalance of this cellular homeostasis, resulting in
427 significant cell proliferation during tumorigenesis (Fig. 9).
428 The formation of the primary cilium has been divided into several distinct phases. It
429 begins with the maturation of the mother centriole, also known as a
430 centriole-to-basal-body transition[9, 41]. DAVs, which are small cytoplasmic vesicles
431 originating from the Golgi and the recycling endosome, accumulate in the vicinity of
432 distal appendages of the mother centriole[25, 42, 43]. Rab8a is localized to
433 cytoplasmic vesicles and the Golgi/trans-Golgi network in growing RPE1 cells, while
434 Rab8-positive vesicles are rapidly redistributed to the mother centriole with binding to
435 Rab11-positive recycling and are endosomes under serum starvation[26, 44]. The
436 EHD1 protein converts these DAVs to form larger ciliary vesicles, which elongate
437 through continuous fusion with Rab8-positive vesicles to produce the primary cilium
438 membrane[25, 30, 40]. Thus, Rab11-positive recycling endosomes, as important
439 transporters, are necessary for primary cilium formation and a centriole-basal-body
440 transition in the early phase. Our study found that CRB3 could bind to some Rab
441 small GTPase family members to significantly participate in Golgi vesicle transport
442 and vesicle organization pathways through mass spectrometry identification. And
443 coexpression and co-IP results showed that CRB3 directly interacted with Rab11 via
444 extracellular domain, which mediated the intracellular trafficking of CRB3 within
445 Rab11-positive endosomes at different cell densities.
446 Unlike motile cilia, primary cilia have only nine outer doublet microtubules without a
447 central pair of microtubules (9+0 structure). Similar to microtubule assembly at
448 microtubule-organizing centers (MTOCs) during mitosis, γ-tubulin, which is a part of
449 γTuRC, is also concentrated in the basal body of the cilium in interphase[45].
450 γ-Tubulin complexes have been shown to form microtubule templates and regulate

451 microtubule nucleation through longitudinal contacts with α-tubulin and β-tubulin[27].
452 The γTuRC consists of multiple copies of γTuSC, which is composed of two copies of
453 γ-tubulin and one each of GCP2 and GCP3. Then, GCP2 and GCP3 interact with
454 GCP4, GCP5 and GCP6 to form γTuRC[46]. Our experiments showed that CRB3
455 knockdown does not affect the expression of the γTuRC-specific proteins GCP3,
456 GCP6 and γ-tubulin but inhibits the interaction between GCP6 and GCP3, resulting in
457 destabilization of γTuRC. Further analysis revealed significant colocalization between
458 GCP6- and Rab11-positive vesicles at low cell density, while at high cell density,
459 GCP6 accumulated at the centrosome together with GCP3. CRB3 knockdown results
460 in the disappearance of this accumulated GCP6. These results indicated that
461 GCP6/Rab11 trafficking vesicles must be transported to the basal body for
462 ciliogenesis. While it is still unclear how CRB3 interferes with γTuRC assembly
463 during primary cilium formation, we hypothesize that Rab11-positive endosomes
464 mediate the intracellular trafficking of CRB3 and that CRB3, as a navigator
465 interacting with CEP290, can navigate GCP6/Rab11 trafficking vesicles to the
466 transition zone for γTuRC assembly in primary cilium formation.
467 CEP290 is considered a centriolar or ciliary protein localized to the centrosomes in
468 dividing cells, the distal mother centriole in quiescent cells, and the transition zone in
469 the primary cilium[47]. *CEP290* mutations are associated with various diseases, such
470 as the devastating blinding disease Leber's Congenital Amaurosis (LCA),
471 nephronophthisis, Senior Løken syndrome (SLS), Joubert syndrome (JS),
472 Bardet-Biedl syndrome (BBS), and lethal Meckel-Gruber syndrome (MGS)[48]. In
473 particular, the phenotypes of CEP290-associated ciliopathies are very similar to those
474 in our *Crb3* knockout mouse model, with lethality and ocular and renal abnormalities.
475 CEP290 knockdown significantly decreased the number of cells with primary cilia,
476 and CEP290 knockout mice showed mislocalization of ciliary proteins in the
477 retinas[49, 50]. Additionally, the depletion of CEP290 disrupts protein trafficking to
478 centrosomes and affects the recruitment of the BBSome and vesicular trafficking in
479 ciliary assembly[51, 52]. Although CEP290 serves as a hub to recruit many ciliary
480 proteins, it has not been reported to be involved in polarized vesicle trafficking or

481 localization. Our study verified that CEP290 could interact with the polarity protein
482 CRB3. CRB3 knockdown disrupts the interaction between CEP290 and
483 Rab11-positive endosomes. Thus, these results validate our hypothesis. Although
484 CRB3 navigates GCP6/Rab11 trafficking vesicles to CEP290, we further need to
485 detect the region of CRB3 interacting with CEP290 and what other cargos are
486 transported by CRB3/Rab11 trafficking vesicles in ciliary assembly.
487 In addition, our results showed that CRB3 knockdown could not activate the Hh
488 signaling pathway with SAG in MCF10A cells. Under untreated conditions, PTCH1
489 located at the ciliary membrane inhibits SMO, and Suppressor of Fused (SuFu)
490 sequesters Gli transcription factors, leading to its degradation. SAG can activate the
491 Hh signaling pathway, resulting in dissociation into the nucleus to regulate the
492 expression of downstream target genes[53]. The Hh signaling pathway mainly
493 regulates cellular growth and differentiation and is abnormal in different types of
494 tumors. Some studies indicate that cilia are double-sided, promoting and preventing
495 cancer development through the Hh signaling pathway *in vivo*. It is thought that cilia
496 deletion could activate SMO to inhibit tumor growth, while promoting carcinogenesis
497 was induced by activated Gli2[54]. Although SAG cannot activate the Hh signaling
498 pathway in CRB3-depleted cells, CRB3 regulation of the carcinogenic process
499 through the ciliary Hh signaling pathway still needs further research. In addition,
500 another canonical Wnt signaling pathway was altered after CRB3 knockdown. The
501 Wnt signaling pathway is an important cascade regulating development and stemness,
502 and aberrant Wnt signaling has been reported in many more cancer entities, especially
503 colorectal cancer[55]. CRB3 downregulated the expression of β-catenin in our study.
504 Thus, CRB3 can affect cilium-related signaling pathways in tumorigenesis.
505 In summary, our study provides novel evidence for the apical polarity protein CRB3
506 in the regulation of viability, mammary and ocular development, and primary cilium
507 formation in germline and conditional knockout mice. CRB3 deletion causes irregular
508 lumen formation and ductal epithelial hyperplasia in mammary epithelial-specific
509 knockout mice. Further study uncovered a new function of CRB3 in directly
510 interacting with Rab11, navigating GCP6/Rab11 trafficking vesicles to CEP290 for

511 γTuRC assembly during ciliogenesis. In addition, CRB3 also participates in regulating
512 cilium-related Hh and Wnt signaling pathways in tumorigenesis. Understanding these
513 polarity protein-mediated vesicle trafficking mechanisms will shed new light on
514 luminal development and tumorigenesis.
515
516
517 **Methods**
518 **Generation of floxed *Crb3* mice.** All animal experiments were verified and approved
519 by the Committee of Institutional Animal Care and Use of Xi'an Jiaotong University.
520 Heterozygous *Crb3*$^{wt/fl}$ mice (C57BL/6J) were generated by Cas9/CRISPR-mediated
521 genome editing (Cyagen Biosciences, Guangzhou, China). The gRNA to *Crb3* and
522 Cas9 mRNA was coinjected into fertilized mouse eggs to generate targeted
523 conditional knockout offspring. The sequences of the *Crb3* gRNA were gRNA1,
524 5'-GGCTGGGTCCACACCTACGGAGG-3'; gRNA2,
525 5'-ACCCACAAAGCCACGCCA GTGGG-3'. Mouse genotyping was screened by
526 PCR with the primers F1, 5'-ACATAAGGCCTTCCGTTAAGCTG-3'; R1, 5'-
527 GTGGATTCGGACCAGTCTGA-3'. *Crb3*$^{wt/fl}$ mice were intercrossed with
528 MMTV-*Cre* mice or CAG-*Cre* mice to generate tissue-specific *Crb3* knockout mice.
529 MMTV-*Cre* mice (FVB), CAG-*Cre* mice (C57BL/6N) and MMTV-PyMT mice (FVB)
530 were purchased from Cyagen Biosciences. All mice were bred in the specific
531 pathogen-free (SPF) animal houses of the Laboratory Animal Center of Xi'an
532 Jiaotong University.
533 Mice were genotyped by using PCR and DNA gel electrophoresis. Genomic DNA
534 from the mouse tail was extracted by using the Mouse Direct PCR Kit (Bimake, TX,
535 USA, #B40015) according to the manufacturer's instructions. The genotyping primers
536 were F3, 5'-TTGAGAGTCTTAAGCAGTCAGGG-3'; R5, 5'-
537 AACCTTTCCCAGGAGTA TGTGAC-3'. PCR results showed that *Crb3*$^{wt/wt}$ was one
538 band with 163 bp, *Crb3*$^{wt/fl}$ was two bands with 228 bp and 163 bp, and *Crb3*$^{fl/fl}$ was
539 one band with 228 bp. The primers for identifying *Cre* alleles were F,
540 5'-TTGAGAGTCTTAAGCAGTCAGGG-3'; R,

541 5'-TTACCACTCCCAGCAAGACAC-3', and amplification with one 247 bp band.
542 The reaction conditions of *Crb3* and *Cre* PCR were as follows: 94°C for 5 min, 94°C
543 for 20 s, 60°C for 30 s, and 72°C for 20 s for 35 cycles.
544 **Mouse mammary gland whole mount analysis.** After mice were euthanized, the
545 inguinal mammary gland tissues were removed intact and fully spread onto slides.
546 Tissues were rapidly fixed in Carnoy's fixative for 2 h at room temperature. Then, the
547 tissues were washed in 70% ethanol solution for 15 min at room temperature and in
548 50 and 30% ethanol and distilled water for 5 min each. Staining was carried out in
549 carmine alum solution at 4°C overnight. After washing with 70% ethanol solution,
550 tissues were washed again in 70, 95 and 100% ethanol for 15 min each. Tissues were
551 cleared in xylene overnight at room temperature and then mounted with neutral
552 balsam. Images were obtained by using a microscope (Leica DMi8, Wetzlar,
553 Germany).
554 **Cell culture and transfection.** MCF10A, MCF7, T47D, MDA-MB-231, HCC1806,
555 T47D, MDA-MB-453 cell lines were purchased from Shanghai Institute of
556 Biochemistry and Cell Biology (Chinese Academy of Sciences, Shanghai, China).
557 MCF10A cells were routinely grown in DMEM/F12 (1:1) media (HyClone, UT, USA)
558 supplemented with 5% horse serum, 20 ng/ml human EGF, 10 μg/ml insulin, and 0.5
559 μg/ml hydrocortisone. MCF7, MDA-MB-231 and MDA-MB-453 cells were cultured
560 in high glucose DMEM media (HyClone, UT, USA) supplemented with 10% FBS
561 (HyClone, UT, USA, #SH30084.03). T47D and HCC1806 cells were grown in
562 RPMI-1640 media (HyClone, UT, USA) supplemented with 10% FBS. All cell lines
563 were incubated in 5% CO_2 at 37°C.
564 siRNAs were purchased from GenePharma company (Shanghai, China). Cultured
565 cells were transfected with siRNAs or plasmids by using Lipofectamine 2000
566 (Invitrogen, CA, USA, #11668-019) following the manufacturer's protocol. The
567 negative control shRNA (NC) and shRNA against CRB3 were packaged into
568 lentivirus as previously described[5, 6].
569 **DNA constructs and stable cell lines.** CRB3 was PCR amplified from RNA
570 extracted from MCF10A cells and cloned into the pCMV-Blank vector (Beyotime,

571 Shanghai, China, D2602) using T4 ligase (NEB, MA, USA). Then, the GFP sequence
572 was inserted between the extracellular and transmembrane CRB3 domains to generate
573 the pCMV-CRB3-GFP vector as described previously[31]. The full-length CRB3
574 (1-120), CRB3 (1-116), CRB3 (1-83), CRB3 (1-58) and CRB3 (1-26) were amplified
575 by PCR from the pCMV-CRB3-GFP vector using specific primers to create EcoR I
576 and Xho I restriction sites and cloned into the pCMV-Blank vector. Full-length was
577 cloned into the lentiviral vector pLVX-TetOne-Puro (Clontech, Takara, #631849).
578 pECMV-3×FLAG-RAB11A was purchased from SinoBiological (Beijing, China).
579 The plasmids of pECMV-3×FLAG-RAB11A[S20V]/[S25N]/[Q70 L] mutants were
580 constructed by using the *Fast* Mutagenesis System (Transgen, Beijing, China,
581 FM111-01).
582 Lentiviruses were produced in HEK293T cells. CRB3-GFP in MCF10A and MCF7
583 cells was generated by using a lentivirus expression system. Screening of stable cell
584 lines used puromycin after lentiviral infection for 72 h.
585 **3D morphogenesis.** The growth factor-reduced Matrigel (Corning, USA, #354230)
586 was added to the four-well chamber slide system (Corning, USA, #177437) and then
587 incubated at 37°C for solidification. MCF10A cells were plated into this chamber
588 slide and cultured in DMEM/F12 (1:1) media (HyClone, UT, USA) supplemented
589 with 2% horse serum, 5 ng/ml human EGF, 10 μg/ml insulin, 0.5 μg/ml
590 hydrocortisone, and 2.5% Matrigel. 3D morphogenesis was photographed using a
591 microscope (Leica DMi8, Wetzlar, Germany) at different time points. 3D MCF10A
592 cells were fixed and stained on day 14 after cell culture.
593 **Immunohistochemistry.** The paraffin-embedded sections of samples were baked,
594 deparaffinized in xylene, and rehydrated sequentially in gradient concentrations of
595 ethanol, sequentially. Then, antigen retrieval was performed in Tris-EDTA buffer (pH
596 9.0) heated to 95°C for 20 min. Endogenous peroxidase activity was reduced in 3%
597 hydrogen peroxide for 10 min at room temperature. Then, 5% goat plasma was used
598 for blocking at 37°C for 30 min, and the sections were incubated with specific
599 primary antibodies overnight at 4°C. Ki67 (Abcam, UK, ab279653), phospho-histone
600 H3 (Abcam, UK, ab267372), cleaved caspase 3 (CST, USA, #9661), GLI1 (CST,

601 USA, #3538), and β-catenin (CST, USA, #8480) were used as primary antibodies. The
602 following steps used biotin-streptavidin HRP detection kits (ZSGB-BIO, China,
603 SP-9001, SP-9002) according to the manufacturer's instructions. The sections were
604 stained with DAB (ZSGB-BIO, China, ZLI-9017), counterstained with hematoxylin,
605 dehydrated in gradient concentrations of ethanol, cleared in xylene, and mounted with
606 neutral balsam, sequentially. Images were obtained by using a slide scanner (Leica
607 SCN400, Wetzlar, Germany).

608 **Immunofluorescence.** Cells were plated on coverslips and fixed in 4%
609 paraformaldehyde for 30 min. Then, the membranes were permeabilized by using 0.2%
610 Triton X-100. The cells were blocked with 5% BSA solution for 1 h at room
611 temperature. Cells were incubated with specific primary antibodies overnight at 4°C.
612 Caspase 3 (CST, USA, #9662S), α-tubulin (CST, USA, #3873), acetylated tubulin
613 (Proteintech, USA, #662001-IG), γ-tubulin (Proteintech, USA, #15176-1-AP),
614 pericentrin (Abcam, UK, ab4448), CRB3 (Sigma, USA, HPA013835), EEA1 (BD,
615 USA, #610456), Rab11 (BD, USA, #610823), and GCP6 (Abcam, UK, ab95172)
616 were used as primary antibodies. The secondary antibodies were Alexa Fluor
617 488-labeled or 594-labeled (Invitrogen, USA, A32731, A32744). DPIA (5 μg/ml) was
618 used for DNA staining, and images were taken by using a confocal microscope (Leica
619 SP5 II, Wetzlar, Germany).

620 **MEFs isolation and maintenance.** The embryos were harvested from
621 *Crb3*$^{wt/fl}$;CAG-Cre mice crosses at E13.5. Head, tail and all innards were removed
622 from these embryos. DNA could be extracted from the tails for genotyping. Then, the
623 body was minced and digested with trypsin in a 37°C incubator for 30 min. Cells
624 were resuspended in MEF media (DME, 10% FBS, 1% penicillin/streptomycin) and
625 plated on 10 cm cell culture dishes with one embryo. They were passaged 1:3 with
626 MEF media for further expansion.

627 **Real-time PCR assay.** Total RNA from cell lines was isolated by using TRIzol
628 reagent (Invitrogen, USA, #15596026), and 5 μg RNA was converted to cDNA with
629 the RevertAid first strand cDNA synthesis kit (Thermo, USA, K1622) according to
630 the manufacturer's instructions. Real-time PCR was prepared with SYBR qPCR

631 Premix (Takara, Japan, RR420L) and then performed with a real-time PCR detection
632 instrument (Bio–Rad CFX96, USA). The primers used for real-time PCR were
633 purchased from Tsingke Biotech (Beijing, China), and the sequences are listed in
634 Table 1. The mRNA expression was normalized to *GAPDH*, and fold changes were
635 calculated by using the ΔΔCt method.

636 **Immunoprecipitation and immunoblotting.** Cultured cells were lysed in RIPA
637 buffer supplemented with protease inhibitors (Roche, NJ, USA). Then, the cell lysates
638 were subjected to SDS–PAGE separation and transferred to PVDF membranes. The
639 membranes were subjected to immunoblot assays using antibodies against CRB3
640 (Santa Cruz, USA, sc-292449), GCP2 (Santa Cruz, USA, sc-377117), GCP3 (Santa
641 Cruz, USA, sc-373758), GCP4 (Santa Cruz, USA, sc-271876), GCP5 (Santa Cruz,
642 USA, sc-365837), GCP6 (Abcam, UK, ab95172), γ-tubulin (Proteintech, USA,
643 #66320-1-Ig), Rab11 (Abcam, UK, ab128913), GFP (Roche, USA, #11814460001),
644 Flag (Sigma, USA, F7425), CEP290 (Santa Cruz, USA, sc-390637), GSK3-β (CST,
645 USA, #12456), β-catenin (CST, USA, #8480), GAPDH (Proteintech, USA,
646 #HRP-6004), and β-actin (Proteintech, USA, #HRP-60008). HRP-conjugated
647 secondary antibodies (CST, USA, #7074, #7076) were incubated at room temperature
648 for 1 h in the dark. Final detection was detected by ECL Plus (Millipore, Germany,
649 WBULS0500). Proteins for the immunoprecipitation assay were lysed with NP40
650 buffer. The cell lysates were detected by a Dynabeads protein G immunoprecipitation
651 kit (Invitrogen, USA, #10007D) according to the manufacturer's instructions. Elution
652 protein complexes were subjected to immunoblot assay.

653 **Protein identification and bioinformatics analyses.** LC−MS/MS analysis was
654 conducted by PTM Bio (Zhejiang, China). Q Exactive^{TM} Plus (Thermo, MA, USA)
655 was used for tandem mass spectrometry data analysis. The Blast2GO program against
656 the UniProt database was used to analyze the functional annotation and classification
657 of the identified proteins. Then, pathway enrichment analysis was enriched by using
658 DAVID tools.

659 **Scanning electron microscope (SEM) observations.** CRB3-GFP and CRB3

knockdown MCF10A cells were plated on culture slides, and doxycycline (Dox) was added to induce the expression of CRB3-GFP. After the cells were fully confluent, the slides were fixed with 4% paraformaldehyde at 4°C overnight and then with 1% osmium tetroxide at 4°C for 1 h. Dehydration was performed at room temperature, and the samples were dried using the critical point drying method. Images were obtained by using a scanning electron microscope (Hitachi TM1000, Japan).

Clinical data. Patient data, breast cancer tissues and adjacent para-cancerous tissues were collected from the First Affiliated Hospital of Xi'an Jiaotong University (Shaanxi, China). All patients signed informed consent forms before surgery. This research was authorized by the Ethics Committee of the First Affiliated Hospital of Xi'an Jiaotong University and conducted in conformity with the Declaration of Helsinki.

Statistics. Statistical analysis was performed using SPSS statistics 23.0 for Windows (IBM, Armonk, USA). All experiments were repeated at least three times. The values are expressed as the mean ± standard deviation (SD). Unpaired Student's *t* test was used to compare the differences between two groups. One-way ANOVA followed by Dunnett's multiple comparisons test was used for multiple comparisons. The χ^2 test was used to assess the significance of the observed frequencies. $P<0.05$ was considered an indicator of statistical significance.

Acknowledgments

This work was supported by grants from the National Natural Science Foundation of China (No. 81872272 and 82173023), Innovation Capability Support Program of Shaanxi (No. 2020TD-046) and Clinical Research Award of the First Affiliated Hospital of Xi'an Jiaotong University (No. XJTU1AF-CRF-2017-007). We are grateful to Prof. Ceshi Chen (Kunming Institute of Zoology, China) and Prof. Yongping Shao (Xi'an Jiaotong University, China) for help in guiding the research. We thank Qi Tian, Lizhe Zhu and Yan Zhou for help with the experiments.

Conflict of interest

The authors declare no conflicts of interest.

Author contributions

P.L. designed the research; B.W., Z.L., T.T, Y.J., Y.S., R.W., H.C., J.L. and P.L. performed the experimental work, and M.Z., X.G., J.L. and S.S. analyzed the data; B.W., Z.L., Y.R. and P.L. wrote the original manuscript. P.L. conceived the study and critically revised the manuscript. All authors read and approved the final manuscript.

Data availability

The datasets used and/or analyzed during the current study are available from the corresponding author on reasonable request.

References

1. Wodarz A, Näthke I. Cell polarity in development and cancer. Nature cell biology. 2007;9(9):1016-24. Epub 2007/09/01. doi: 10.1038/ncb433. PubMed PMID: 17762893.

2. McCaffrey LM, Macara IG. Epithelial organization, cell polarity and tumorigenesis. Trends in cell biology. 2011;21(12):727-35. Epub 2011/07/26. doi: 10.1016/j.tcb.2011.06.005. PubMed PMID: 21782440.

3. Etienne-Manneville S. Polarity proteins in migration and invasion. Oncogene. 2008;27(55):6970-80. Epub 2008/11/26. doi: 10.1038/onc.2008.347. PubMed PMID: 19029938.

4. Elsum I, Yates L, Humbert PO, Richardson HE. The Scribble-Dlg-Lgl polarity module in development and cancer: from flies to man. Essays in biochemistry. 2012;53:141-68. Epub 2012/08/30. doi: 10.1042/bse0530141. PubMed PMID: 22928514.

5. Li P, Wang Y, Mao X, Jiang Y, Liu J, Li J, et al. CRB3 downregulation confers breast cancer stem cell traits through TAZ/β-catenin. Oncogenesis. 2017;6(4):e322. Epub 2017/04/25. doi: 10.1038/oncsis.2017.24. PubMed PMID: 28436991; PubMed Central PMCID: PMCPMC5520500.

6. Mao X, Li P, Wang Y, Liang Z, Liu J, Li J, et al. CRB3 regulates contact inhibition by activating the Hippo pathway in mammary epithelial cells. Cell death & disease. 2017;8(1):e2546. Epub 2017/01/13. doi: 10.1038/cddis.2016.478. PubMed PMID: 28079891; PubMed Central PMCID: PMCPMC5386381.

7. Mao X, Li P, Ren Y, Li J, Zhou C, Yang J, et al. Cell polarity protein CRB3 is an independent favorable prognostic factor for clear cell renal cell carcinoma. International journal

725 of oncology. 2015;46(2):657-66. doi: 10.3892/ijo.2014.2763. PubMed PMID:
726 WOS:000347671200025.
727 8. Karp CM, Tan TT, Mathew R, Nelson D, Mukherjee C, Degenhardt K, et al. Role of the
728 polarity determinant crumbs in suppressing mammalian epithelial tumor progression. Cancer
729 research. 2008;68(11):4105-15. Epub 2008/06/04. doi: 10.1158/0008-5472.Can-07-6814.
730 PubMed PMID: 18519669; PubMed Central PMCID: PMCPMC2696887.
731 9. Sánchez I, Dynlacht BD. Cilium assembly and disassembly. Nature cell biology.
732 2016;18(7):711-7. Epub 2016/06/29. doi: 10.1038/ncb3370. PubMed PMID: 27350441;
733 PubMed Central PMCID: PMCPMC5079433.
734 10. Reiter JF, Leroux MR. Genes and molecular pathways underpinning ciliopathies. Nature
735 reviews Molecular cell biology. 2017;18(9):533-47. Epub 2017/07/13. doi:
736 10.1038/nrm.2017.60. PubMed PMID: 28698599; PubMed Central PMCID:
737 PMCPMC5851292.
738 11. Kim J, Dabiri S, Seeley ES. Primary cilium depletion typifies cutaneous melanoma in situ
739 and malignant melanoma. PloS one. 2011;6(11):e27410. Epub 2011/11/19. doi:
740 10.1371/journal.pone.0027410. PubMed PMID: 22096570; PubMed Central PMCID:
741 PMCPMC3214062.
742 12. Menzl I, Lebeau L, Pandey R, Hassounah NB, Li FW, Nagle R, et al. Loss of primary cilia
743 occurs early in breast cancer development. Cilia. 2014;3:7. Epub 2014/07/06. doi:
744 10.1186/2046-2530-3-7. PubMed PMID: 24987519; PubMed Central PMCID:
745 PMCPMC4076761.
746 13. Basten SG, Willekers S, Vermaat JS, Slaats GG, Voest EE, van Diest PJ, et al. Reduced

747 cilia frequencies in human renal cell carcinomas versus neighboring parenchymal tissue. Cilia.
748 2013;2(1):2. Epub 2013/02/02. doi: 10.1186/2046-2530-2-2. PubMed PMID: 23369289;
749 PubMed Central PMCID: PMCPMC3564780.
750 14. Seeley ES, Carrière C, Goetze T, Longnecker DS, Korc M. Pancreatic cancer and
751 precursor pancreatic intraepithelial neoplasia lesions are devoid of primary cilia. Cancer
752 research. 2009;69(2):422-30. Epub 2009/01/17. doi: 10.1158/0008-5472.Can-08-1290.
753 PubMed PMID: 19147554; PubMed Central PMCID: PMCPMC2629528.
754 15. Hassounah NB, Nagle R, Saboda K, Roe DJ, Dalkin BL, McDermott KM. Primary cilia are
755 lost in preinvasive and invasive prostate cancer. PloS one. 2013;8(7):e68521. Epub
756 2013/07/12. doi: 10.1371/journal.pone.0068521. PubMed PMID: 23844214; PubMed Central
757 PMCID: PMCPMC3699526.
758 16. Bazellières E, Aksenova V, Barthélémy-Requin M, Massey-Harroche D, Le Bivic A. Role
759 of the Crumbs proteins in ciliogenesis, cell migration and actin organization. Seminars in cell &
760 developmental biology. 2018;81:13-20. Epub 2017/10/24. doi: 10.1016/j.semcdb.2017.10.018.
761 PubMed PMID: 29056580.
762 17. Fan S, Fogg V, Wang Q, Chen XW, Liu CJ, Margolis B. A novel Crumbs3 isoform
763 regulates cell division and ciliogenesis via importin beta interactions. The Journal of cell
764 biology. 2007;178(3):387-98. Epub 2007/07/25. doi: 10.1083/jcb.200609096. PubMed PMID:
765 17646395; PubMed Central PMCID: PMCPMC2064851.
766 18. Fan S, Hurd TW, Liu CJ, Straight SW, Weimbs T, Hurd EA, et al. Polarity proteins control
767 ciliogenesis via kinesin motor interactions. Current biology : CB. 2004;14(16):1451-61. Epub
768 2004/08/25. doi: 10.1016/j.cub.2004.08.025. PubMed PMID: 15324661.

769 19. Whiteman EL, Fan S, Harder JL, Walton KD, Liu CJ, Soofi A, et al. Crumbs3 is essential
770 for proper epithelial development and viability. Molecular and cellular biology.
771 2014;34(1):43-56. Epub 2013/10/30. doi: 10.1128/mcb.00999-13. PubMed PMID: 24164893;
772 PubMed Central PMCID: PMCPMC3911272.
773 20. Ye X, Tam WL, Shibue T, Kaygusuz Y, Reinhardt F, Ng Eaton E, et al. Distinct EMT
774 programs control normal mammary stem cells and tumour-initiating cells. Nature.
775 2015;525(7568):256-60. Epub 2015/09/04. doi: 10.1038/nature14897. PubMed PMID:
776 26331542; PubMed Central PMCID: PMCPMC4764075.
777 21. Soule HD, Maloney TM, Wolman SR, Peterson WD, Jr., Brenz R, McGrath CM, et al.
778 Isolation and characterization of a spontaneously immortalized human breast epithelial cell
779 line, MCF-10. Cancer research. 1990;50(18):6075-86. Epub 1990/09/25. PubMed PMID:
780 1975513.
781 22. Halsne R, Tandberg JI, Lobert VH, Østby GC, Thoen E, Ropstad E, et al. Effects of
782 perfluorinated alkyl acids on cellular responses of MCF-10A mammary epithelial cells in
783 monolayers and on acini formation in vitro. Toxicol Lett. 2016;259:95-107. Epub 2016/08/12.
784 doi: 10.1016/j.toxlet.2016.08.004. PubMed PMID: 27511595.
785 23. Jonassen JA, San Agustin J, Follit JA, Pazour GJ. Deletion of IFT20 in the mouse kidney
786 causes misorientation of the mitotic spindle and cystic kidney disease. The Journal of cell
787 biology. 2008;183(3):377-84. Epub 2008/11/05. doi: 10.1083/jcb.200808137. PubMed PMID:
788 18981227; PubMed Central PMCID: PMCPMC2575779.
789 24. Martin-Belmonte F, Perez-Moreno M. Epithelial cell polarity, stem cells and cancer.
790 Nature reviews Cancer. 2011;12(1):23-38. Epub 2011/12/16. doi: 10.1038/nrc3169. PubMed

791 PMID: 22169974.

792 25. Lu Q, Insinna C, Ott C, Stauffer J, Pintado PA, Rahajeng J, et al. Early steps in primary
793 cilium assembly require EHD1/EHD3-dependent ciliary vesicle formation. Nature cell biology.
794 2015;17(3):228-40. Epub 2015/02/17. doi: 10.1038/ncb3109. PubMed PMID: 25686250;
795 PubMed Central PMCID: PMCPMC4344897.

796 26. Westlake CJ, Baye LM, Nachury MV, Wright KJ, Ervin KE, Phu L, et al. Primary cilia
797 membrane assembly is initiated by Rab11 and transport protein particle II (TRAPPII)
798 complex-dependent trafficking of Rabin8 to the centrosome. Proceedings of the National
799 Academy of Sciences of the United States of America. 2011;108(7):2759-64. Epub 2011/01/29.
800 doi: 10.1073/pnas.1018823108. PubMed PMID: 21273506; PubMed Central PMCID:
801 PMCPMC3041065 R.H.S., and P.K.J. are employees of Genentech, Inc.

802 27. Kollman JM, Merdes A, Mourey L, Agard DA. Microtubule nucleation by γ-tubulin
803 complexes. Nature reviews Molecular cell biology. 2011;12(11):709-21. Epub 2011/10/14. doi:
804 10.1038/nrm3209. PubMed PMID: 21993292; PubMed Central PMCID: PMCPMC7183383.

805 28. Liu P, Zupa E, Neuner A, Böhler A, Loerke J, Flemming D, et al. Insights into the
806 assembly and activation of the microtubule nucleator γ-TuRC. Nature. 2020;578(7795):467-71.
807 Epub 2019/12/20. doi: 10.1038/s41586-019-1896-6. PubMed PMID: 31856152.

808 29. Farache D, Jauneau A, Chemin C, Chartrain M, Rémy MH, Merdes A, et al. Functional
809 Analysis of γ-Tubulin Complex Proteins Indicates Specific Lateral Association via Their
810 N-terminal Domains. The Journal of biological chemistry. 2016;291(44):23112-25. Epub
811 2016/10/30. doi: 10.1074/jbc.M116.744862. PubMed PMID: 27660388; PubMed Central
812 PMCID: PMCPMC5087730.

813 30. Knödler A, Feng S, Zhang J, Zhang X, Das A, Peränen J, et al. Coordination of Rab8 and
814 Rab11 in primary ciliogenesis. Proceedings of the National Academy of Sciences of the United
815 States of America. 2010;107(14):6346-51. Epub 2010/03/24. doi: 10.1073/pnas.1002401107.
816 PubMed PMID: 20308558; PubMed Central PMCID: PMCPMC2851980.
817 31. Djuric I, Siebrasse JP, Schulze U, Granado D, Schlüter MA, Kubitscheck U, et al. The
818 C-terminal domain controls the mobility of Crumbs 3 isoforms. Biochimica et biophysica acta.
819 2016;1863(6 Pt A):1208-17. Epub 2016/03/16. doi: 10.1016/j.bbamcr.2016.03.008. PubMed
820 PMID: 26975581.
821 32. Craige B, Tsao CC, Diener DR, Hou Y, Lechtreck KF, Rosenbaum JL, et al. CEP290
822 tethers flagellar transition zone microtubules to the membrane and regulates flagellar protein
823 content. The Journal of cell biology. 2010;190(5):927-40. Epub 2010/09/08. doi:
824 10.1083/jcb.201006105. PubMed PMID: 20819941; PubMed Central PMCID:
825 PMCPMC2935561.
826 33. Casenghi M, Meraldi P, Weinhart U, Duncan PI, Körner R, Nigg EA. Polo-like kinase 1
827 regulates Nlp, a centrosome protein involved in microtubule nucleation. Developmental cell.
828 2003;5(1):113-25. Epub 2003/07/11. doi: 10.1016/s1534-5807(03)00193-x. PubMed PMID:
829 12852856.
830 34. Li P, Feng C, Chen H, Jiang Y, Cao F, Liu J, et al. Elevated CRB3 expression suppresses
831 breast cancer stemness by inhibiting β-catenin signalling to restore tamoxifen sensitivity.
832 Journal of cellular and molecular medicine. 2018;22(7):3423-33. Epub 2018/03/31. doi:
833 10.1111/jcmm.13619. PubMed PMID: 29602199; PubMed Central PMCID:
834 PMCPMC6010813.

835 35. Thiery JP, Acloque H, Huang RY, Nieto MA. Epithelial-mesenchymal transitions in
836 development and disease. Cell. 2009;139(5):871-90. Epub 2009/12/01. doi:
837 10.1016/j.cell.2009.11.007. PubMed PMID: 19945376.
838 36. Varelas X, Samavarchi-Tehrani P, Narimatsu M, Weiss A, Cockburn K, Larsen BG, et al.
839 The Crumbs complex couples cell density sensing to Hippo-dependent control of the
840 TGF-β-SMAD pathway. Developmental cell. 2010;19(6):831-44. Epub 2010/12/15. doi:
841 10.1016/j.devcel.2010.11.012. PubMed PMID: 21145499.
842 37. Charrier LE, Loie E, Laprise P. Mouse Crumbs3 sustains epithelial tissue morphogenesis
843 in vivo. Scientific reports. 2015;5:17699. Epub 2015/12/04. doi: 10.1038/srep17699. PubMed
844 PMID: 26631503; PubMed Central PMCID: PMCPMC4668553.
845 38. Herranz-Martín S, Jimeno D, Paniagua AE, Velasco A, Lara JM, Aijón J, et al.
846 Immunocytochemical evidence of the localization of the Crumbs homologue 3 protein (CRB3)
847 in the developing and mature mouse retina. PloS one. 2012;7(11):e50511. Epub 2012/12/12.
848 doi: 10.1371/journal.pone.0050511. PubMed PMID: 23226298; PubMed Central PMCID:
849 PMCPMC3511585.
850 39. Arya P, Rainey MA, Bhattacharyya S, Mohapatra BC, George M, Kuracha MR, et al. The
851 endocytic recycling regulatory protein EHD1 Is required for ocular lens development.
852 Developmental biology. 2015;408(1):41-55. Epub 2015/10/13. doi:
853 10.1016/j.ydbio.2015.10.005. PubMed PMID: 26455409; PubMed Central PMCID:
854 PMCPMC4688215.
855 40. Rainey MA, George M, Ying G, Akakura R, Burgess DJ, Siefker E, et al. The endocytic
856 recycling regulator EHD1 is essential for spermatogenesis and male fertility in mice. BMC Dev

857 Biol. 2010;10:37. Epub 2010/04/03. doi: 10.1186/1471-213x-10-37. PubMed PMID: 20359371;
858 PubMed Central PMCID: PMCPMC2856533.
859 41. Kobayashi T, Dynlacht BD. Regulating the transition from centriole to basal body. The
860 Journal of cell biology. 2011;193(3):435-44. Epub 2011/05/04. doi: 10.1083/jcb.201101005.
861 PubMed PMID: 21536747; PubMed Central PMCID: PMCPMC3087006.
862 42. Kobayashi T, Kim S, Lin YC, Inoue T, Dynlacht BD. The CP110-interacting proteins
863 Talpid3 and Cep290 play overlapping and distinct roles in cilia assembly. The Journal of cell
864 biology. 2014;204(2):215-29. Epub 2014/01/15. doi: 10.1083/jcb.201304153. PubMed PMID:
865 24421332; PubMed Central PMCID: PMCPMC3897186.
866 43. Schmidt KN, Kuhns S, Neuner A, Hub B, Zentgraf H, Pereira G. Cep164 mediates
867 vesicular docking to the mother centriole during early steps of ciliogenesis. The Journal of cell
868 biology. 2012;199(7):1083-101. Epub 2012/12/21. doi: 10.1083/jcb.201202126. PubMed
869 PMID: 23253480; PubMed Central PMCID: PMCPMC3529528.
870 44. Das A, Guo W. Rabs and the exocyst in ciliogenesis, tubulogenesis and beyond. Trends
871 in cell biology. 2011;21(7):383-6. Epub 2011/05/10. doi: 10.1016/j.tcb.2011.03.006. PubMed
872 PMID: 21550243; PubMed Central PMCID: PMCPMC3128673.
873 45. Guichard P, Laporte MH, Hamel V. The centriolar tubulin code. Seminars in cell &
874 developmental biology. 2021. Epub 2021/12/14. doi: 10.1016/j.semcdb.2021.12.001. PubMed
875 PMID: 34896019.
876 46. Liu P, Würtz M, Zupa E, Pfeffer S, Schiebel E. Microtubule nucleation: The waltz between
877 γ-tubulin ring complex and associated proteins. Current opinion in cell biology. 2021;68:124-31.
878 Epub 2020/11/16. doi: 10.1016/j.ceb.2020.10.004. PubMed PMID: 33190097.

879 47. Chen HY, Kelley RA, Li T, Swaroop A. Primary cilia biogenesis and associated retinal
880 ciliopathies. Seminars in cell & developmental biology. 2021;110:70-88. Epub 2020/08/05. doi:
881 10.1016/j.semcdb.2020.07.013. PubMed PMID: 32747192; PubMed Central PMCID:
882 PMCPMC7855621.
883 48. Drivas TG, Bennett J. CEP290 and the primary cilium. Advances in experimental
884 medicine and biology. 2014;801:519-25. Epub 2014/03/26. doi:
885 10.1007/978-1-4614-3209-8_66. PubMed PMID: 24664739.
886 49. Tsang WY, Bossard C, Khanna H, Peränen J, Swaroop A, Malhotra V, et al. CP110
887 suppresses primary cilia formation through its interaction with CEP290, a protein deficient in
888 human ciliary disease. Developmental cell. 2008;15(2):187-97. Epub 2008/08/13. doi:
889 10.1016/j.devcel.2008.07.004. PubMed PMID: 18694559; PubMed Central PMCID:
890 PMCPMC3987787.
891 50. Chang B, Khanna H, Hawes N, Jimeno D, He S, Lillo C, et al. In-frame deletion in a novel
892 centrosomal/ciliary protein CEP290/NPHP6 perturbs its interaction with RPGR and results in
893 early-onset retinal degeneration in the rd16 mouse. Human molecular genetics.
894 2006;15(11):1847-57. Epub 2006/04/25. doi: 10.1093/hmg/ddl107. PubMed PMID: 16632484;
895 PubMed Central PMCID: PMCPMC1592550.
896 51. Kim J, Krishnaswami SR, Gleeson JG. CEP290 interacts with the centriolar satellite
897 component PCM-1 and is required for Rab8 localization to the primary cilium. Human
898 molecular genetics. 2008;17(23):3796-805. Epub 2008/09/06. doi: 10.1093/hmg/ddn277.
899 PubMed PMID: 18772192; PubMed Central PMCID: PMCPMC2722899.
900 52. Stowe TR, Wilkinson CJ, Iqbal A, Stearns T. The centriolar satellite proteins Cep72 and

901 Cep290 interact and are required for recruitment of BBS proteins to the cilium. Molecular
902 biology of the cell. 2012;23(17):3322-35. Epub 2012/07/07. doi: 10.1091/mbc.E12-02-0134.
903 PubMed PMID: 22767577; PubMed Central PMCID: PMCPMC3431927.
904 53. Wheway G, Nazlamova L, Hancock JT. Signaling through the Primary Cilium. Frontiers in
905 cell and developmental biology. 2018;6:8. Epub 2018/02/24. doi: 10.3389/fcell.2018.00008.
906 PubMed PMID: 29473038; PubMed Central PMCID: PMCPMC5809511.
907 54. Wong SY, Seol AD, So PL, Ermilov AN, Bichakjian CK, Epstein EH, Jr., et al. Primary cilia
908 can both mediate and suppress Hedgehog pathway-dependent tumorigenesis. Nature
909 medicine. 2009;15(9):1055-61. Epub 2009/08/25. doi: 10.1038/nm.2011. PubMed PMID:
910 19701205; PubMed Central PMCID: PMCPMC2895420.
911 55. Zhan T, Rindtorff N, Boutros M. Wnt signaling in cancer. Oncogene. 2017;36(11):1461-73.
912 Epub 2016/09/13. doi: 10.1038/onc.2016.304. PubMed PMID: 27617575; PubMed Central
913 PMCID: PMCPMC5357762.
914
915

916 **Figure 1.** *Crb3* knockout mice exhibit smaller sizes and ocular abnormalities, and
917 mammary epithelial cell-specific *Crb3* knockout leads to ductal epithelial hyperplasia
918 and promotes tumorigenesis.
919 A, B. Representative whole bodies (A) and eyes (B) from littermate *Crb3*$^{fl/fl}$,
920 *Crb3*$^{wt/fl}$;CAG-*Cre* and *Crb3*$^{fl/fl}$;CAG-*Cre* mice at 4 weeks old. C. Representative
921 mammary whole mounts from littermate *Crb3*$^{fl/fl}$ and *Crb3*$^{fl/fl}$;MMTV-*Cre* mice at 8
922 weeks old with Carmine-alum staining. (scale bars, 200 μm) D, E. Quantification of
923 the average number of TEBs (n=10) and bifurcated TEBs (n=10) in littermate *Crb3*$^{fl/fl}$
924 and *Crb3*$^{fl/fl}$;MMTV-*Cre* mice at 8 weeks old. F. Representative images of mammary
925 glands in littermate *Crb3*$^{fl/fl}$ and *Crb3*$^{fl/fl}$;MMTV-*Cre* mice stained with H&E. (scale
926 bars, 50 μm) G. Representative images of primary tumors stained with H&E in
927 PyMT-WT and PyMT-cKO-*Crb3* mice at 9 weeks old. (scale bars, left 500 μm, right
928 50 μm) Magnified areas of boxed sections are shown in the right panels. Bars
929 represent the means ± SD; Unpaired Student's *t* test, ***$P<0.001$.
930
931 **Figure 2.** CRB3 knockdown inhibits acinar formation of mammary epithelial cells in
932 a 3D culture system.
933 A. Representative effect of CRB3 on acinar formation in the 3D culture system at
934 days 3, 6, 9 and 14. (Magnified areas of marked arrows are shown in the lower right
935 corner) B-D. Quantification of the average number, diameter and aberration of acini
936 (n=10). E. Immunofluorescence showing apoptosis during lumen formation. Caspase
937 3 (red), α-tubulin (green), and DNA (blue). F. Immunofluorescence showing the
938 mitotic spindle orientation during lumen formation. α-Tubulin (green) and DNA
939 (blue). G, H. Quantification of division angle. I. Immunohistochemical analyses of
940 Ki67, phospho-histone H3 and cleaved caspase 3 in primary tumors from PyMT-WT
941 and PyMT-cKO-*Crb3* mice at 9 weeks old. (positive cells marked by arrows) Scale
942 bars, 25 μm, bars represent means ± SD; Unpaired Student's *t* test, * $P<0.5$, **
943 $P<0.01$, ***$P<0.001$.
944
945 **Figure 3.** CRB3 alters primary cilium formation in mammary cells, mammary ductal

946 lumen and renal tubule from *Crb3*$^{fl/fl}$;CAG-*Cre* mice.

947 A. C. Representative images of immunofluorescent staining of primary cilium
948 formation with CRB3 knockdown in MCF10A cells and CRB3 conditional
949 overexpression upon dox induction in MCF7 cells. Acetylated tubulin (red), γ-tubulin
950 (green), and DNA (blue). (primary cilium marked by arrows; scale bars, 10 μm) B. D.
951 Quantification of the proportion of cells with primary cilium formation and the length
952 of the primary cilium (n=10). E. Representative scanning electron microscope images
953 of primary cilium formation with CRB3 knockdown and conditional overexpression
954 in MCF10A cells. (primary cilium marked by arrows; scale bars, 50 μm) F.
955 Quantification of the proportion of cells with primary cilium formation (n=10). G. H.
956 Representative immunofluorescent staining of primary cilium formation in the
957 mammary ductal lumen and renal tubule from *Crb3*$^{fl/fl}$ and *Crb3*$^{fl/fl}$;CAG-*Cre* mice,
958 respectively. Acetylated tubulin (red), γ-tubulin (green), and DNA (blue). (n=10; scale
959 bars, 25 μm) Bars represent the means ± SD; Unpaired Student's *t* test, *$P<0.05$,
960 ***$P<0.001$.

961

962 **Figure 4.** CRB3 localizes to the basal body of the primary cilium.

963 A. Immunofluorescence showing the colocalization of exogenous CRB3 with
964 centrosomes in MCF10A cells. Pericentrin, a marker of centrosome (red), CRB3-GFP
965 (green), and DNA (blue). (Colocalization marked by arrows; scale bars, 10 μm) B.
966 Quantification of the proportion of cells with pericentrin and exogenous CRB3
967 colocalization (n=10). (bars represent the means ± SD) C. Another colocalization of
968 endogenous CRB3 with the basal body in MCF10A cells. γ-Tubulin is a marker of the
969 centrosome and basal body of the primary cilium (green), CRB3 (red), and DNA
970 (blue). (Colocalization marked by arrows; scale bars, 10 μm) D. Corresponding
971 fluorescence intensity profile across a section of the array, as indicated by the dashed
972 white line in (C). E. Double immunostaining displaying the colocalization of CRB3
973 with the primary cilium in MCF10A cells. Acetylated tubulin (green), CRB3 (red),
974 and DNA (blue). (Colocalization marked by arrows; scale bars, 10 μm) F.
975 Fluorescence 3D reconstruction of CRB3 and primary cilium colocalization.

976 Acetylated tubulin (red), CRB3 (green), and DNA (blue).

977

978 **Figure 5.** CRB3 trafficking is mediated by Rab11-positive endosomes, and CRB3
979 knockdown destabilizes γTuRC assembly during ciliogenesis.
980 A. Pathway aggregation analysis of CRB3 binding proteins identified by mass
981 spectrometry in MCF10A cells. B. Table of some Rab small GTPase family members
982 and centriolar proteins identified as CRB3 binding proteins. C. Immunofluorescence
983 showing the colocalization of CRB3 with EEA1-, CD63-, and Rab11-positive
984 endosomes in MCF10A cells. EEA1, CD63, Rab11 (green), CRB3 (red), and DNA
985 (blue). (scale bars, 10 μm) D. Quantification of the proportion of cells with these
986 markers and CRB3 colocalization (n=10). E. Western blots showing the levels of
987 CRB3 in MCF10A cells treated with dynasore at different cell densities. F. Structure
988 diagram of γTuRC (γ-tubulin ring complex). G. Immunoblot analysis of the effect of
989 CRB3 on γTuRC molecules in MCF10A cells. H. Coimmunoprecipitation showing
990 the interacting proteins with GCP6 in MCF10A cells with CRB3 knockdown. I.
991 Representative images of immunofluorescent staining of GCP3 and GCP6
992 colocalization in MCF10A cells with the corresponding fluorescence intensity profile.
993 GCP3 (red), GCP6 (green), and DNA (blue). (scale bars, 10 μm) J. Comparison of
994 cytoplasmic extracts from MCF10A cells and cells with CRB3 knockdown after
995 fractionation in sucrose gradients. The γTuSC sedimentation was mainly in fractions 3,
996 and γTuRC sedimentation was mainly in fractions 6. Bars represent the means ± SD;
997 Unpaired Student's *t* test, ***P<0.001.

998

999 **Figure 6.** CRB3 directly interacts with Rab11.
1000 A. Coimmunoprecipitation of CRB3 with Rab11, GCP6 and GCP3 in MCF10A cells.
1001 B. Coimmunoprecipitation of Rab11 with CRB3, GCP6 and GCP3 in MCF10A cells.
1002 C. Coimmunoprecipitation of Rab11 with GCP6 in control and CRB3 knockdown
1003 MCF10A cells. D. Schematic diagram of CRB3 domains. E. Diagram truncations of
1004 CRB3-GFP fusion proteins with serial C-terminal deletions. F. Domain mapping of
1005 CRB3-GFP for Flag-Rab11a binding. Flag antibody co-IP of the full-length

1006 CRB3-GFP and truncations of CRB3-GFP with Flag-Rab11a were cotransfected into
1007 HEK293 cells for 48 h. Immunoblot analysis was performed using GFP and Flag
1008 antibodies. G. Coimmunoprecipitation of Rab11 mutant variants with full-length
1009 CRB3-GFP. Flag antibody co-IP of the full-length CRB3-GFP with Flag-Rab11aWT,
1010 Flag-Rab11a[Q70L], Flag-Rab11a[S20V] and Flag-Rab11a[S25N] were cotransfected
1011 into HEK293 cells for 48 h. Immunoblot analysis was performed using GFP and Flag
1012 antibodies. Bars represent the means ± SD; Unpaired Student's *t* test, *$P<0.05$.
1013
1014 **Figure 7.** CRB3 navigates GCP6/Rab11 trafficking vesicles to the basal body of the
1015 primary cilium.
1016 A. Coimmunoprecipitation of exogenous CRB3 with Rab11, GCP6, GCP3 and
1017 CEP290 in MCF10A cells. B. Coimmunoprecipitation of Rab11 with exogenous
1018 CRB3, GCP6, GCP3 and CEP290 in MCF10A cells. C. Coimmunoprecipitation of
1019 Rab11 with GCP6 and CEP290 in control and CRB3 knockdown MCF10A cells. D.
1020 Representative immunofluorescent images of GCP6 and γ-tubulin colocalization of
1021 the basal body foci in MCF10A cells with CRB3 knockdown. γ-Tubulin (green),
1022 GCP6 (red), and DNA (blue). (Colocalization marked by arrows; scale bars, 25 μm) E.
1023 Representative immunofluorescent images of Rab11 and γ-tubulin colocalization of
1024 the basal body foci in MEF cells from *Crb3*$^{fl/fl}$ and *Crb3*$^{fl/fl}$;CAG-*Cre* mice. γ-tubulin
1025 (green), Rab11 (red), and DNA (blue). Foci marked by arrows; scale bars, 25 μm.
1026 Bars represent the means ± SD; Unpaired Student's *t* test, ***$P<0.001$.
1027
1028 **Figure 8.** Defects in CRB3 expression inhibit ciliary assembly in breast cancer tissues,
1029 and activate the Wnt signaling pathway in mammary cells and PyMT mouse model.
1030 A. Representative immunofluorescent images of CRB3 in breast cancer tissues (n=50).
1031 CRB3 (green) and DNA (blue). (scale bars, 25 μm) B. Representative
1032 immunofluorescent images of the primary cilium in breast cancer tissues (n=50).
1033 Acetylated tubulin (red), γ-tubulin (green), and DNA (blue). (scale bars, 10 μm) C.
1034 Quantification of the proportion of cells with primary cilium formation in breast
1035 cancer tissues (n=50). D. Representative immunofluorescent images of CRB3 and

1036 γ-tubulin colocalization in adjacent paracarcinoma tissues. CRB3 (green), γ-tubulin
1037 (red), and DNA (blue). (scale bars, 25 μm) E. Quantification of the proportion of
1038 MFC10A cells with SMO translocation after CRB3 knockdown (n=6). F. Real-time
1039 quantitative PCR showing the relative mRNA expression of GLI1 upon SAG
1040 treatment in CRB3-depleted MFC10A cells (n=6). G. Immunoblot analyses of the
1041 effect of CRB3 on the molecules of the Wnt signaling pathway in mammary cells. H.
1042 I. Immunohistochemical analyses of GLI1 and β-catenin in primary tumors from
1043 PyMT-WT and PyMT-cKO-*Crb3* mice at 9 weeks old, respectively. (scale bars, 25
1044 μm) Bars represent the means ± SD; Unpaired Student's *t* test, ***$P<0.001$.
1045
1046 **Figure 9.** Schematic model of CRB3 regulating ciliary assembly.
1047 Graphic summary of prominent phenotypes observed after CRB3 deletion. CRB3 is
1048 localized on apical epithelial surfaces and participates in tight junction formation to
1049 maintain contact inhibition and cell homeostasis in quiescence. Inside the cell,
1050 Rab11-positive endosomes mediate the intracellular trafficking of CRB3, and CRB3
1051 navigates GCP6/Rab11 trafficking vesicles to CEP290. Then, GCP6 is involved in
1052 normal γTuRC assembly in ciliogenesis. In CRB3 deletion cells, the primary cilium
1053 does not assemble properly, and the Wnt signaling pathway is activated through
1054 β-catenin upregulation and nuclear localization, but the Hh signaling pathway fails to
1055 be activated. This cellular imbalance is disrupted, leading to tumorigenesis. γTuRC,
1056 γ-tubulin ring complex; TJ, tight junction; EE, early endosome; LE, late endosome.
1057

1058 **Supplementary Figure 1.** Generation of *Crb3* knockout mice by using the Cre-loxP
1059 system.
1060 A. Schematic representation of the strategy for loxP sequence insertion and PCR
1061 genotyping. The loxP sites (gray arrow) flanked either side of exon 3 (orange) in the
1062 Crb3 gene. The primer pair F3&R5 and F4&R6 were used to distinguish the alleles. B.
1063 Southern blot analysis of a positive ES cell clone confirmed homologous
1064 recombination. The genomic DNA from ES cell clones and wild-type cells was
1065 digested with Avr II or Sac I and hybridized with a 5' external probe or 3' internal
1066 probe. C. PCR identification of mouse genotyping showing *Crb3*$^{wt/wt}$, *Crb3*$^{wt/fl}$ and
1067 *Crb3*$^{fl/fl}$ alleles. D. Crb3 expression was detected by immunoblotting in mammary
1068 gland tissues in *Crb3*$^{fl/fl}$ and *Crb3*$^{fl/fl}$;MMTV-*Cre* mice at 8 weeks old. E. Real-time
1069 quantitative PCR showing the relative mRNA expression of *Crb3* in mammary gland
1070 tissues (n=10). F. Crb3 expression was assessed by using immunohistochemistry in
1071 mammary gland tissues. The mammary epithelial cells were marked by areas of white
1072 dotted lines. (scale bars, 50 μm) Bars represent the means ± SD; Unpaired Student's *t*
1073 test, ***P<0.001.
1074
1075 **Supplementary Figure 2.** CRB3 knockdown promotes proliferation of mammary
1076 epithelial cells, and overexpression promotes apoptosis of breast cancer.
1077 A. B. Immunoblot and real-time quantitative PCR analysis of CRB3 knockout
1078 efficiency in MCF10A cells. C. MCF10A proliferation assay for six successive days.
1079 D. Cell cycle showing the distribution of MCF10A cells. E. Quantification of the cell
1080 cycle distribution. F.G.H. Apoptosis of MCF7, T47D, and MDA-MB-453 breast
1081 cancer cells with CRB3 overexpression and quantification of apoptotic cells. Bars
1082 represent the means ± SD; Unpaired Student's *t* test, * P<0.05, **P<0.01.
1083
1084 **Supplementary Figure 3.** CRB3 alters primary cilium formation in MEFs from
1085 *Crb3*$^{fl/fl}$;CAG-*Cre* mice.
1086 A. Representative immunofluorescent staining of primary cilium formation in MEFs
1087 from *Crb3*$^{fl/fl}$ and *Crb3*$^{fl/fl}$;CAG-*Cre* mice. Acetylated tubulin (red), γ-tubulin (green),

1088 and DNA (blue). (scale bars, 10 μm) B. Quantification of the proportion of cells with
1089 primary cilium formation (n=10). Bars represent the means ± SD; Unpaired Student's
1090 *t* test, ***P<0.001.
1091
1092 **Supplementary Figure 4.** The effect of CRB3 on a series of ciliogenesis-related
1093 genes and Rab11 expression.
1094 A. Quantification of the mRNA expression of genes encoding markers of centriole or
1095 primary cilium, BB components, IFT-A and IFT-B anterograde transport (normalized
1096 to GAPDH). B. Coomassie blue staining showing the gel electrophoresis of
1097 exogenous CRB3 immunoprecipitated precipitates. C. Immunoblot analysis of the
1098 effect of CRB3 on Rab11 in MCF10A cells. Bars represent the means ± SD; Unpaired
1099 Student's *t* test
1100
1101 **Supplementary Figure 5.** CRB3 knockdown disturbed the colocalization of GCP6
1102 and Rab11, and Rab11 knockdown caused primary cilium defects.
1103 A. Representative immunofluorescent staining of the colocalization between Rab11
1104 and GCP6 in MCF10A cells. GCP6 (red), Rab11 (green), and DNA (blue). (scale bars,
1105 20 μm) B. Fluorescence colocalization analysis in (A). C. Quantification of the
1106 proportion of cells with Rab11 and GCP6 colocalization. D. Representative images of
1107 immunofluorescent staining of primary cilium formation with Rab11 knockdown in
1108 MCF10A cells. Acetylated tubulin (red), γ-tubulin (green), and DNA (blue). (primary
1109 cilium marked by arrows; scale bars, 20 μm) E. Quantification of the proportion of
1110 cells with primary cilium formation. F. Immunoblot analysis of Rab11 knockout
1111 efficiency in MCF10A cells. Bars represent the means ± SD; Unpaired Student's *t* test,
1112 **P<0.01, ***P<0.001.
1113

A

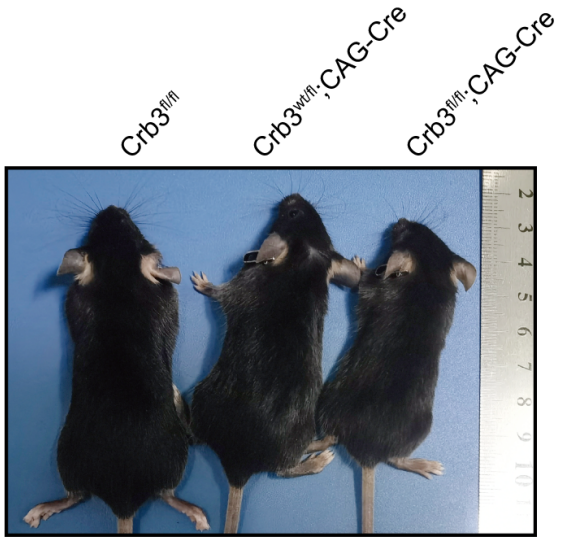
Crb3fl/fl
Crb3wt/fl;CAG-Cre
Crb3fl/fl;CAG-Cre

B

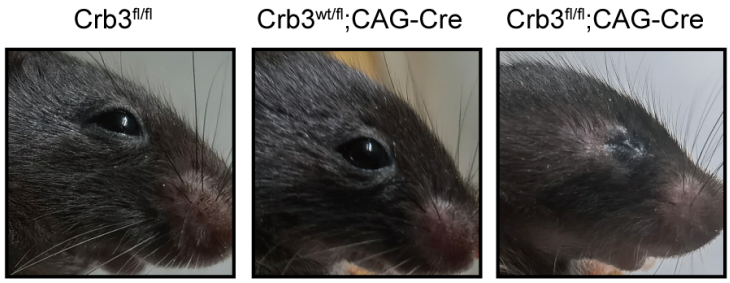
Crb3fl/fl
Crb3wt/fl;CAG-Cre
Crb3fl/fl;CAG-Cre

C

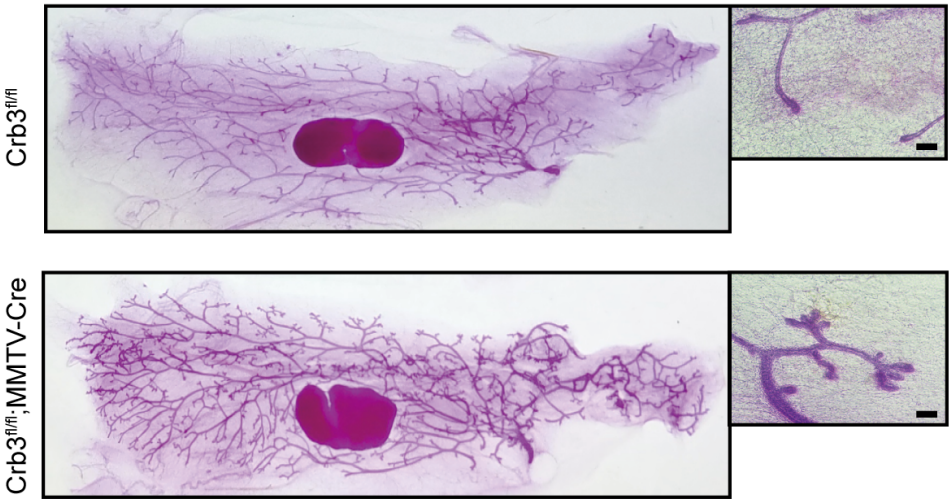
Crb3fl/fl
Crb3fl/fl;MMTV-Cre

D

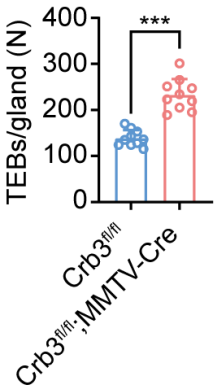
TEBs/gland (N)
400
300
200
100
0
***
Crb3fl/fl
Crb3fl/fl;MMTV-Cre

E

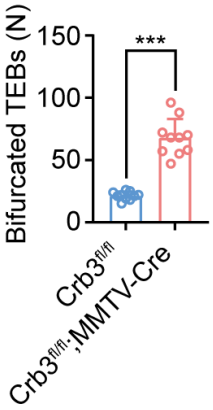
Bifurcated TEBs (N)
150
100
50
0
***
Crb3fl/fl
Crb3fl/fl;MMTV-Cre

F

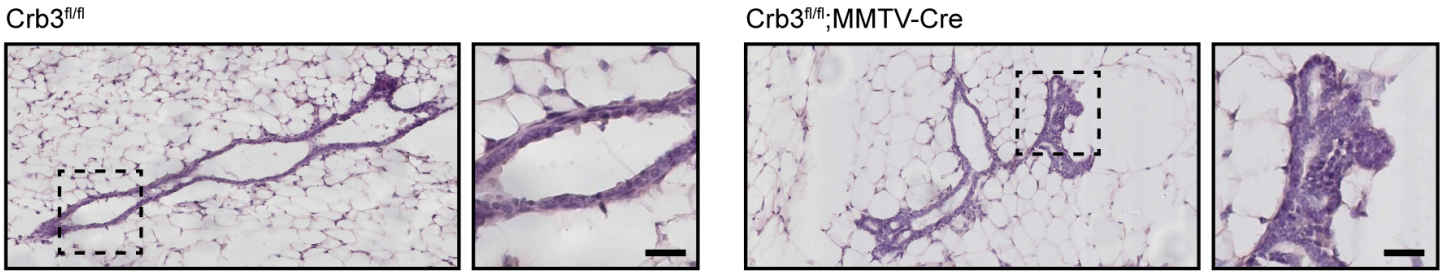
Crb3fl/fl
Crb3fl/fl;MMTV-Cre

G

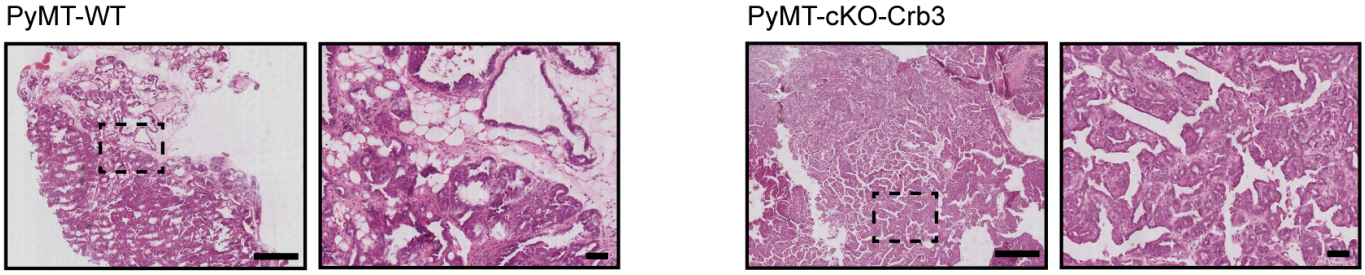
PyMT-WT
PyMT-cKO-Crb3

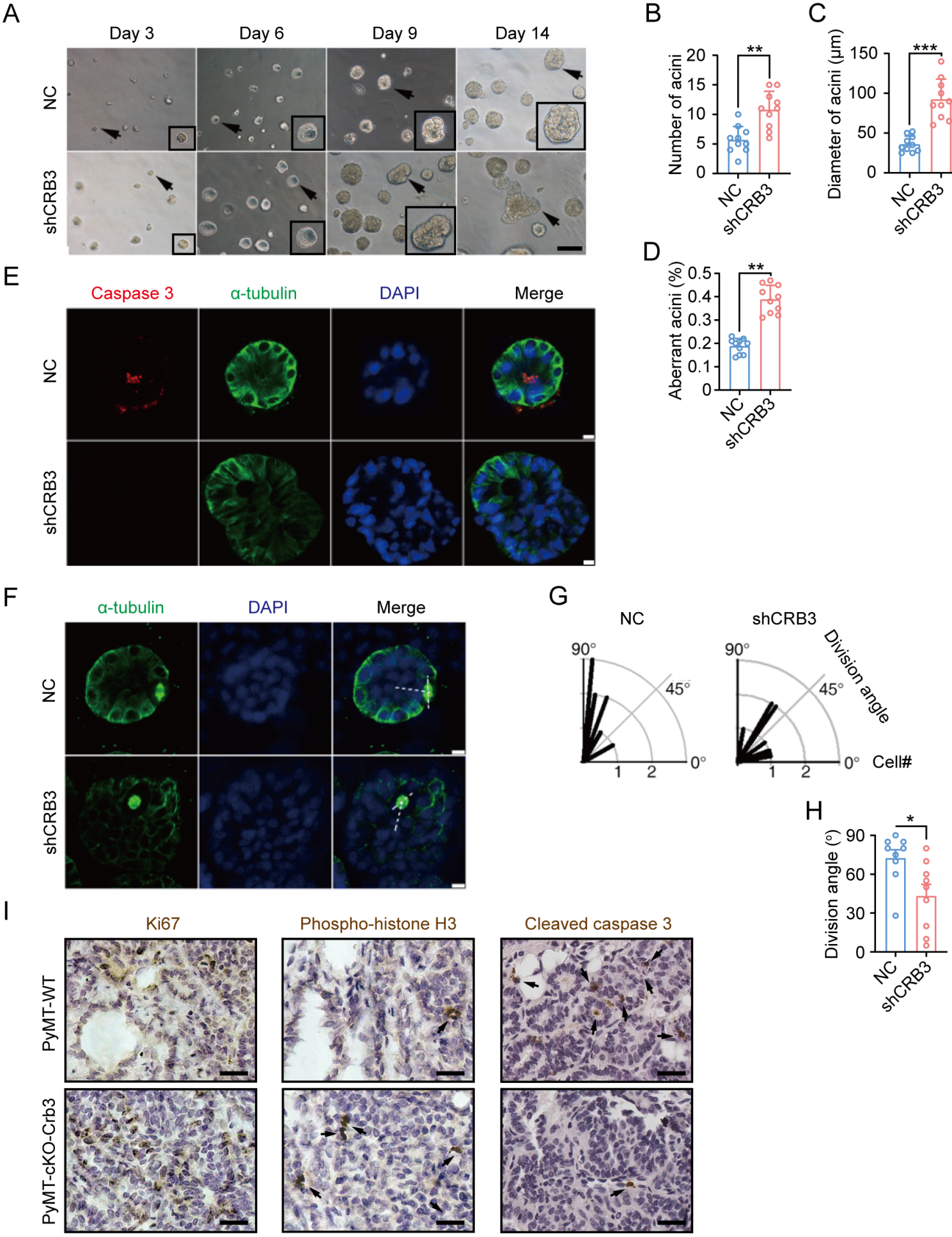
A
Day 3
Day 6
Day 9
Day 14
NC
shCRB3
B
Number of acini
20
15
10
5
0
**
NC
shCRB3
C
Diameter of acini (μm)
150
100
50
0
***
NC
shCRB3
D
Aberrant acini (%)
0.5
0.4
0.3
0.2
0.1
0
**
NC
shCRB3
E
Caspase 3
α-tubulin
DAPI
Merge
NC
shCRB3
F
α-tubulin
DAPI
Merge
NC
shCRB3
G
NC
shCRB3
90°
45°
0°
1
2
Division angle
Cell#
H
Division angle (°)
90
60
30
0
*
NC
shCRB3
I
Ki67
Phospho-histone H3
Cleaved caspase 3
PyMT-WT
PyMT-cKO-Crb3

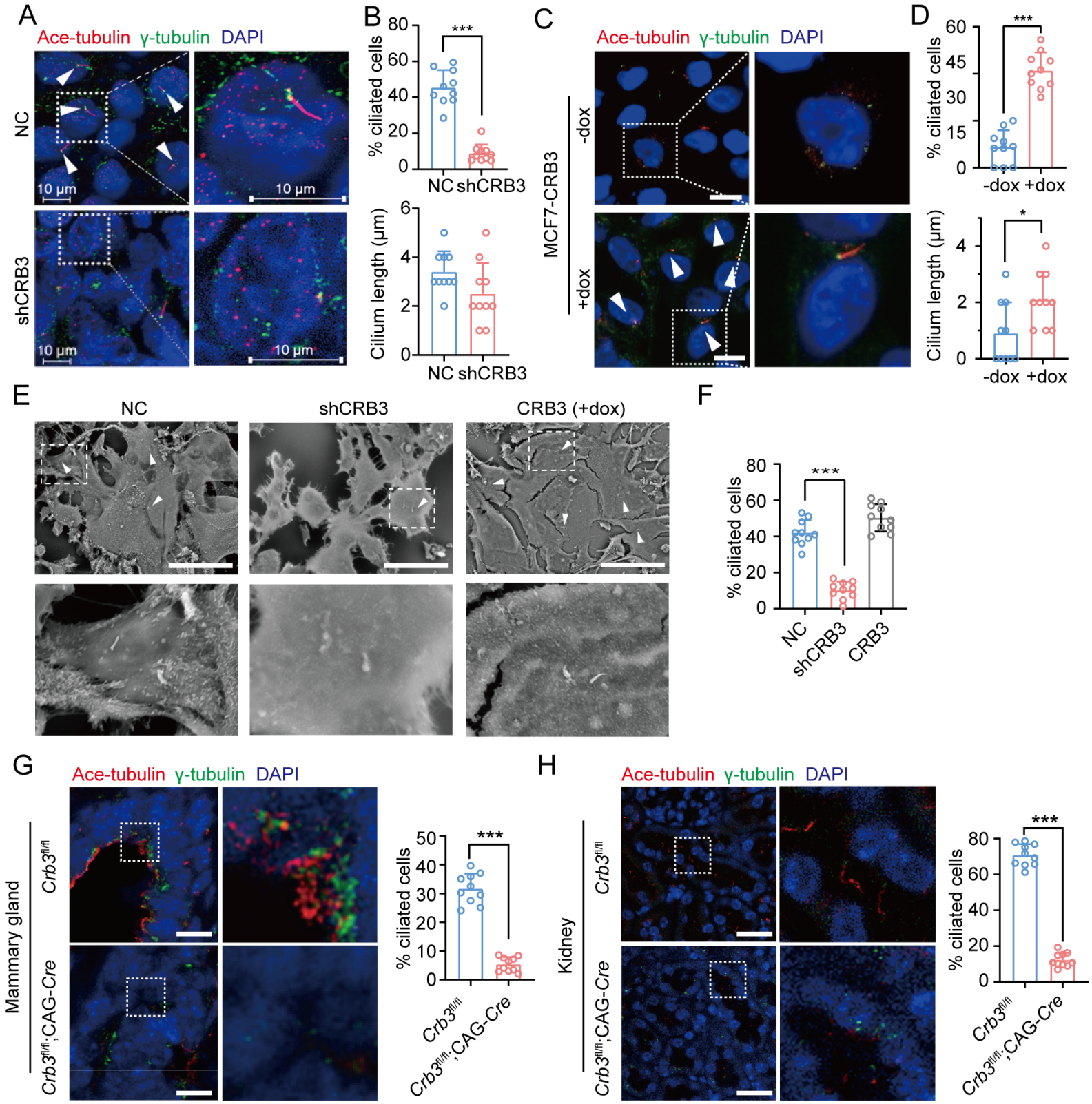
A
Ace-tubulin γ-tubulin DAPI
NC
shCRB3
10 μm
B
% ciliated cells
***
NC shCRB3
Cilium length (μm)
C
Ace-tubulin γ-tubulin DAPI
MCF7-CRB3
-dox
+dox
D
% ciliated cells
***
-dox +dox
Cilium length (μm)
*
E
NC
shCRB3
CRB3 (+dox)
F
% ciliated cells
***
NC
shCRB3
CRB3
G
Ace-tubulin γ-tubulin DAPI
Mammary gland
Crb3fl/fl
Crb3fl/fl;CAG-Cre
% ciliated cells
***
H
Ace-tubulin γ-tubulin DAPI
Kidney
Crb3fl/fl
Crb3fl/fl;CAG-Cre
% ciliated cells
***

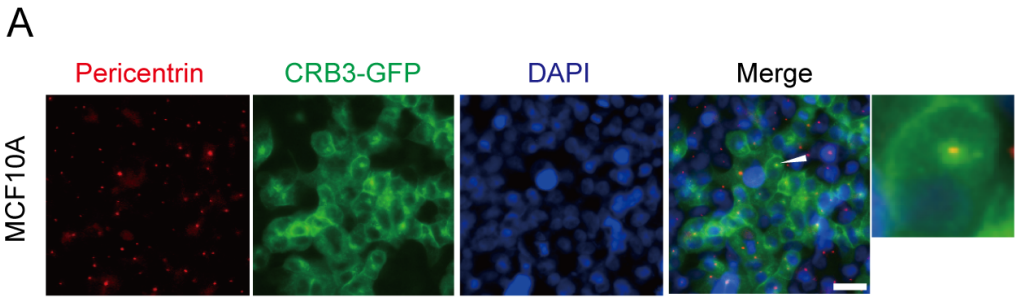
A
Pericentrin
CRB3-GFP
DAPI
Merge
MCF10A

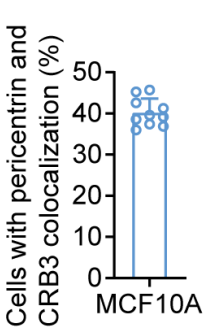
B
Cells with pericentrin and CRB3 colocalization (%)
50
40
30
20
10
0
MCF10A

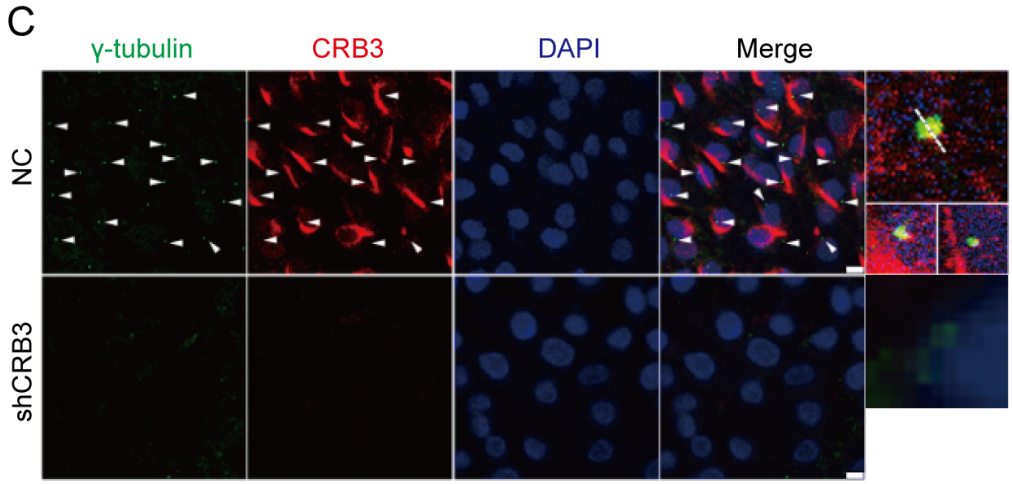
C
γ-tubulin
CRB3
DAPI
Merge
NC
shCRB3

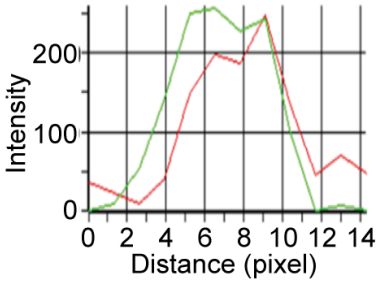
D
Intensity
200
100
0
0 2 4 6 8 10 12 14
Distance (pixel)

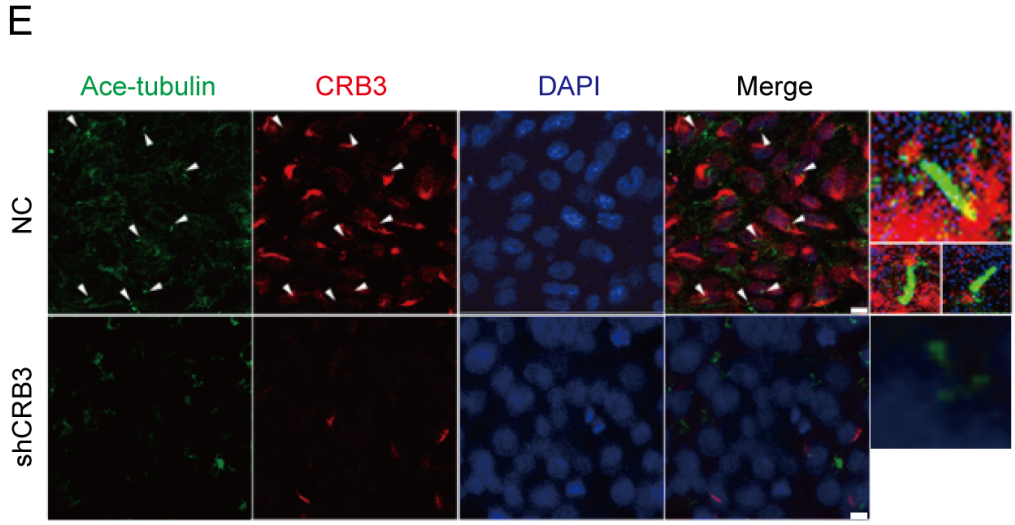
E
Ace-tubulin
CRB3
DAPI
Merge
NC
shCRB3

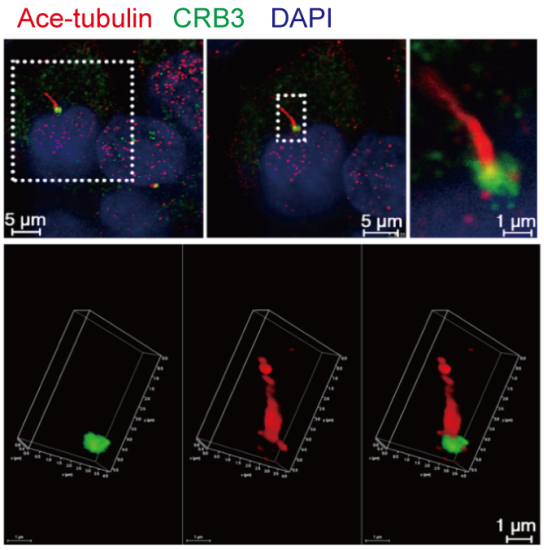
F
Ace-tubulin
CRB3
DAPI
5 μm
5 μm
1 μm
1 μm

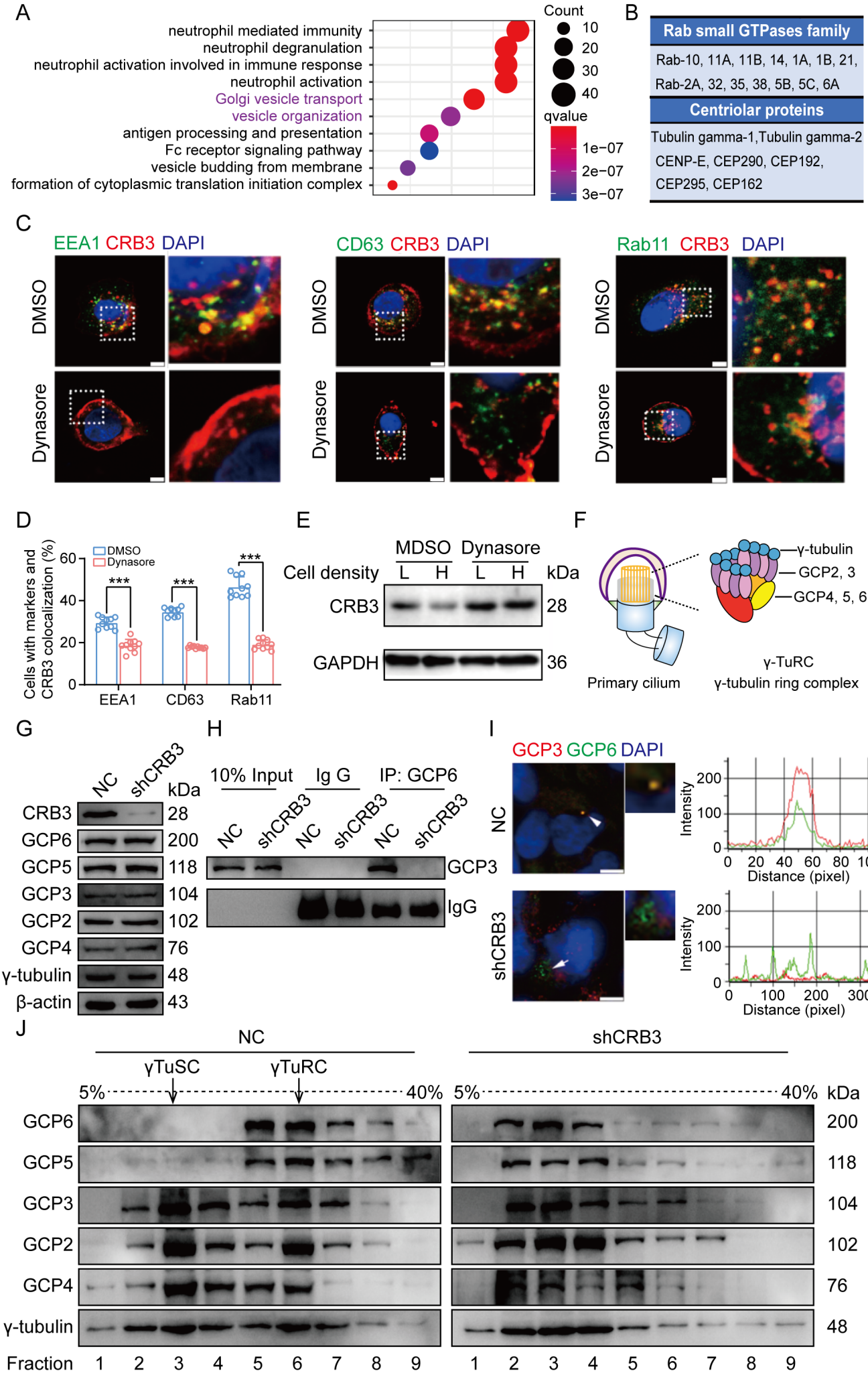
A
neutrophil mediated immunity
neutrophil degranulation
neutrophil activation involved in immune response
neutrophil activation
Golgi vesicle transport
vesicle organization
antigen processing and presentation
Fc receptor signaling pathway
vesicle budding from membrane
formation of cytoplasmic translation initiation complex
Count
10
20
30
40
qvalue
1e−07
2e−07
3e−07
B
Rab small GTPases family
Rab-10, 11A, 11B, 14, 1A, 1B, 21, Rab-2A, 32, 35, 38, 5B, 5C, 6A
Centriolar proteins
Tubulin gamma-1,Tubulin gamma-2 CENP-E, CEP290, CEP192, CEP295, CEP162
C
EEA1 CRB3 DAPI
CD63 CRB3 DAPI
Rab11 CRB3 DAPI
DMSO
Dynasore
D
Cells with markers and CRB3 colocalization (%)
DMSO
Dynasore
***
EEA1
CD63
Rab11
E
MDSO
Dynasore
Cell density
L
H
L
H
kDa
CRB3
28
GAPDH
36
F
γ-tubulin
GCP2, 3
GCP4, 5, 6
Primary cilium
γ-TuRC
γ-tubulin ring complex
G
NC
shCRB3
kDa
CRB3
28
GCP6
200
GCP5
118
GCP3
104
GCP2
102
GCP4
76
γ-tubulin
48
β-actin
43
H
10% Input
Ig G
IP: GCP6
NC
shCRB3
GCP3
IgG
I
GCP3 GCP6 DAPI
NC
shCRB3
Intensity
Distance (pixel)
J
NC
shCRB3
γTuSC
γTuRC
5%
40%
kDa
GCP6
200
GCP5
118
GCP3
104
GCP2
102
GCP4
76
γ-tubulin
48
Fraction
1
2
3
4
5
6
7
8
9

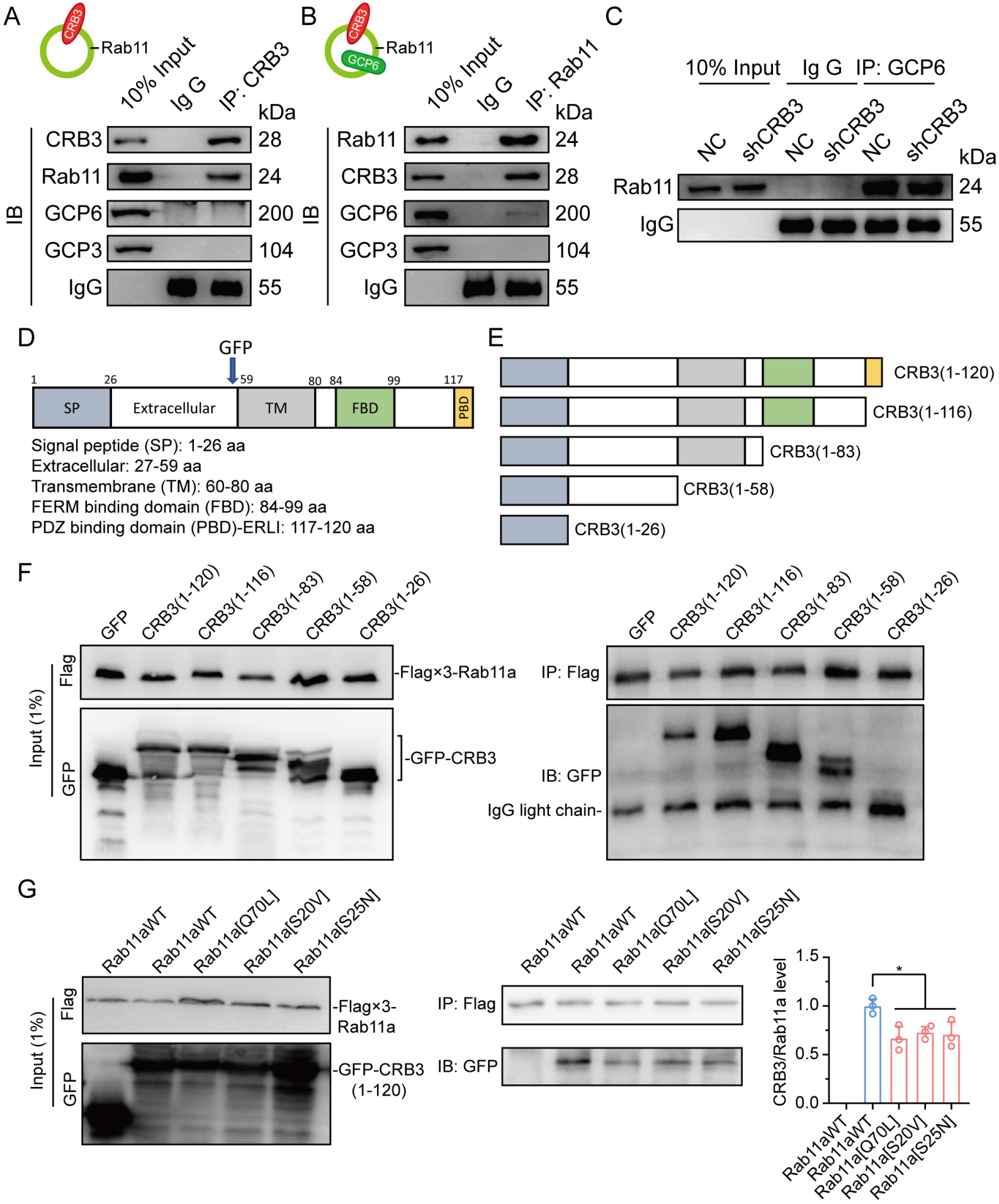
A
CRB3
Rab11
10% Input
Ig G
IP: CRB3
kDa
IB
CRB3 28
Rab11 24
GCP6 200
GCP3 104
IgG 55
B
CRB3
GCP6
Rab11
10% Input
Ig G
IP: Rab11
kDa
IB
Rab11 24
CRB3 28
GCP6 200
GCP3 104
IgG 55
C
10% Input
Ig G
IP: GCP6
NC
shCRB3
NC
shCRB3
NC
shCRB3
kDa
Rab11 24
IgG 55
D
GFP
1
26
59
80
84
99
117
SP
Extracellular
TM
FBD
PBD
Signal peptide (SP): 1-26 aa
Extracellular: 27-59 aa
Transmembrane (TM): 60-80 aa
FERM binding domain (FBD): 84-99 aa
PDZ binding domain (PBD)-ERLI: 117-120 aa
E
CRB3(1-120)
CRB3(1-116)
CRB3(1-83)
CRB3(1-58)
CRB3(1-26)
F
GFP
CRB3(1-120)
CRB3(1-116)
CRB3(1-83)
CRB3(1-58)
CRB3(1-26)
Input (1%)
Flag
GFP
-Flag×3-Rab11a
-GFP-CRB3
IP: Flag
IB: GFP
IgG light chain-
G
Rab11aWT
Rab11aWT
Rab11a[Q70L]
Rab11a[S20V]
Rab11a[S25N]
Input (1%)
Flag
GFP
-Flag×3-Rab11a
-GFP-CRB3 (1-120)
IP: Flag
IB: GFP
CRB3/Rab11a level
1.5
1.0
0.5
0.0
*

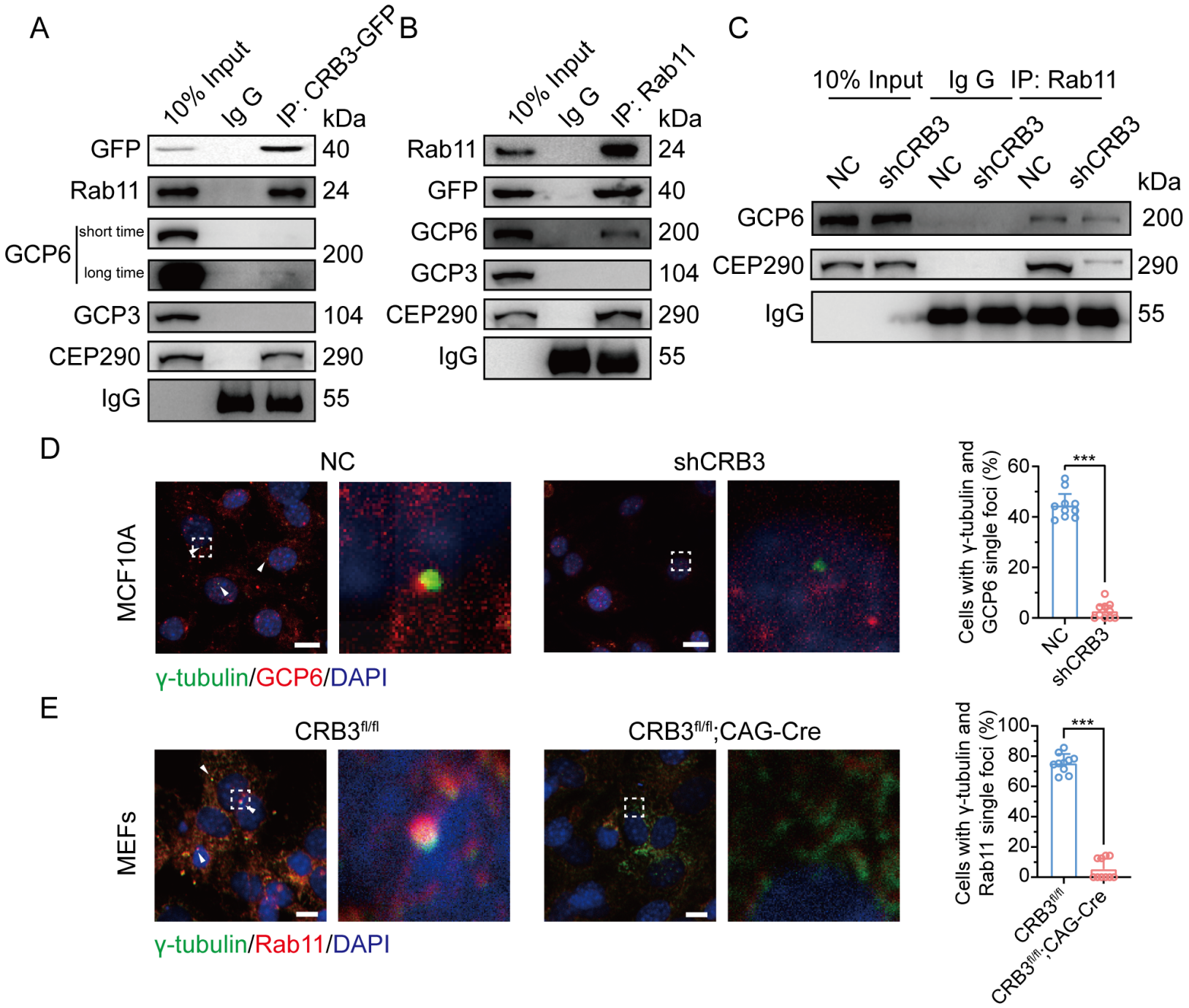
A
10% Input
Ig G
IP: CRB3-GFP
kDa
GFP
40
Rab11
24
GCP6
short time
long time
200
GCP3
104
CEP290
290
IgG
55
B
10% Input
Ig G
IP: Rab11
kDa
Rab11
24
GFP
40
GCP6
200
GCP3
104
CEP290
290
IgG
55
C
10% Input
Ig G
IP: Rab11
NC
shCRB3
NC
shCRB3
NC
shCRB3
kDa
GCP6
200
CEP290
290
IgG
55
D
NC
shCRB3
MCF10A
γ-tubulin/GCP6/DAPI
Cells with γ-tubulin and GCP6 single foci (%)
60
40
20
0
***
NC
shCRB3
E
CRB3fl/fl
CRB3fl/fl;CAG-Cre
MEFs
γ-tubulin/Rab11/DAPI
Cells with γ-tubulin and Rab11 single foci (%)
100
80
60
40
20
0
***
CRB3fl/fl
CRB3fl/fl;CAG-Cre

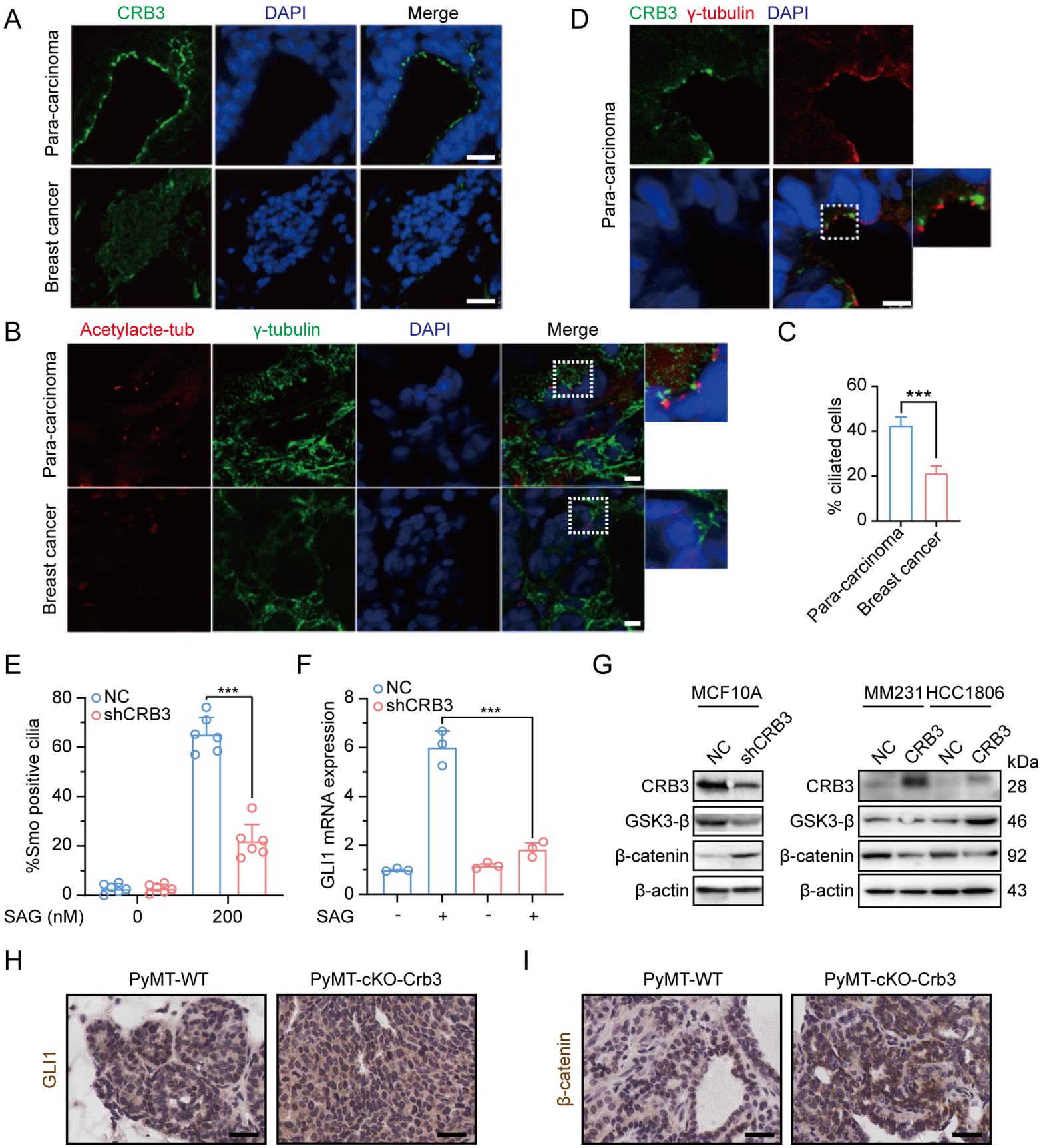
A
CRB3
DAPI
Merge
Para-carcinoma
Breast cancer
D
CRB3
γ-tubulin
DAPI
Para-carcinoma
B
Acetylacte-tub
γ-tubulin
DAPI
Merge
Para-carcinoma
Breast cancer
C
% ciliated cells
60
40
20
0
***
Para-carcinoma
Breast cancer
E
%Smo positive cilia
80
60
40
20
0
NC
shCRB3
***
SAG (nM)
0
200
F
GLI1 mRNA expression
8
6
4
2
0
NC
shCRB3
***
SAG
-
+
-
+
G
MCF10A
MM231
HCC1806
NC
shCRB3
NC
CRB3
NC
CRB3
kDa
CRB3
GSK3-β
β-catenin
β-actin
28
46
92
43
H
PyMT-WT
PyMT-cKO-Crb3
GLI1
I
PyMT-WT
PyMT-cKO-Crb3
β-catenin

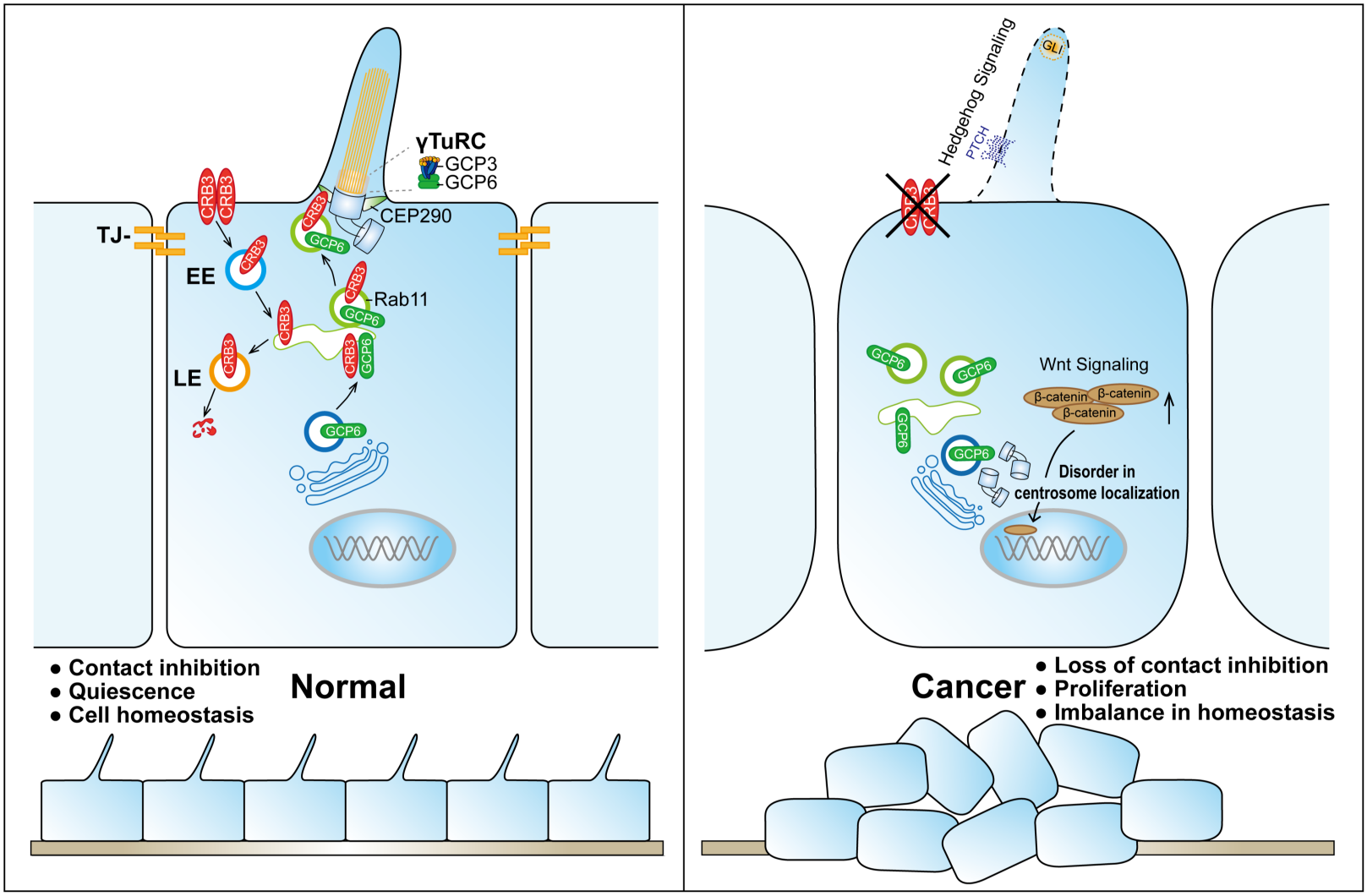
γTuRC
GCP3
GCP6
CEP290
TJ-
CRB3
EE
LE
Rab11
GCP6
• Contact inhibition
• Quiescence
• Cell homeostasis
Normal
Hedgehog Signaling
GLI
PTCH
Wnt Signaling
β-catenin
Disorder in
centrosome localization
Cancer
• Loss of contact inhibition
• Proliferation
• Imbalance in homeostasis